Manuscript submitted to *Weather and Forecasting*

Mesoscale Snowfall Prediction and Verification in Mountainous Terrain

MELANIE WETZEL*, MICHAEL MEYERS[+], RANDOLPH BORYS*, RAY MCANELLY[#], WILLIAM COTTON[#], ANDREW ROSSI*, PAUL FRISBIE[+], DAVID NADLER[+], DOUGLAS LOWENTHAL, STEPHEN COHN[&] AND WILLIAM BROWN[&]
**Desert Research Institute, Reno, Nevada*
[+]*National Weather Service, Grand Junction, Colorado*
[#]*Colorado State University, Fort Collins, Colorado*
[&]*National Center for Atmospheric Research, Boulder, Colorado*

ABSTRACT

Short term forecasting of precipitation often relies on meteorological radar coverage to provide information on the intensity, extent and motion of approaching mesoscale features. However, in significant portions of mountainous regions, radar coverage is lacking due to topographic blocking, and the absence of radar signatures in sections of the radar scan produces uncertain or even misleading information to the public and operational forecasters. In addition, echo characteristics within the radar volume scan are often influenced by the vertical extent and type of precipitation. Each of these conditions limits the opportunity for accurate snowfall prediction and studies of precipitation climatology. To improve both short-term forecasting and post-event verification studies, much greater use can be made of specifically sited surface observations, tailored graphical output from mesoscale models, satellite remote sensing, and case study knowledge of local topographic influences. In this paper, methods to support snowfall forecasts and verification in radar-limited mountainous terrain are demonstrated which include: matching the output parameters and graphics from high-resolution mesoscale models to surface mesonets and snowfall observations ; analysis of continuous and event-based measurements of snow density ; application of multispectral satellite data for verification and trend analysis; and characterization of orographic influences in different winter storm scenarios. The advantages of improved wintertime quantitative precipitation forecasting (QPF) in mountain regions include public safety responsibilities that are critical to National Weather Service (NWS) operations, and are relevant to any mountainous region with radar scan limitations or during periods of radar data outages.

1. Introduction

Many regions of the Intermountain West states have restricted radar coverage, due to the complex terrain, that causes uncertainty and bias in precipitation analysis and short-term (0-12 hour) forecasting. In addition, the lack of observed precipitation patterns leads to gaps in knowledge of mesoscale precipitation climatology that might otherwise aid QPF analysis for time scales longer than 12 hours. Technique development for quantitative snowfall forecasts in orographic terrain is needed, particularly when radar data coverage is degraded by beam blockage. As with satellite imagery, time lapse animations of radar imagery are used whenever possible to anticipate and verify the evolution of storm events. Operational forecasters with local knowledge of radar scan limitations can often recognize how precipitation echo patterns change due to the effects of topography on detectable scan volume. This is particularly true in winter when snowfall is generated from more stratiform cloud systems rather than deep convection.

Since the public has wide access to radar scan graphics, without an experienced eye they may assume that no precipitation exists and disregard short-term precipitation forecasts that impact their decision-making for road or private air travel. Improved interpretation can be provided the public by NWS statements and broadcast weather information, focusing both on the reason for limited radar coverage and the use of other sources to fill the gap for nowcasting and short-term forecasting of precipitation. In geographic areas with limited radar coverage, these other sources of information become critical to forecast verification and trend analysis, for the operational forecast office as well as the general public. Quantitative forecasting of snowfall, in terms of physical depth accumulation, also limited by uncertainty in the density of the falling snow. Many forecast applications (such as highway maintenance, traffic warnings, avalanche control, ski area operations) are more sensitive to accurate prediction of physical snow depth accumulation than snow water equivalent (SWE). Previous studies of fallen snow density indicate the wide variety of snow densities encountered (Judson and Doesken, 2000), and the role of many factors related to in-cloud microphysics and sub-cloud transformation (Roebber *et al.*, 2002).

In general, mountainous regions provide enhanced precipitation rates and accumulations due to orographic uplift. The rate of snowfall accumulation during winter precipitation events is directly related to the efficiency of snow growth processes, and these processes include both kinematic forcing associated with orographic uplift as well as the microphysical structure

conducive to rapid crystal growth and settling. Heggli and Rauber (1988) have shown that much of the supercooled liquid water which contributes to heavy snowfall is typically located in the lowest kilometer above the terrain, and Reinking *et al.* (2000) describe the important process by which ice crystals generated from higher elevations in "seeder" cloud regions grow rapidly by accretion in the "feeder" cloud below. The near-infrared image channel on the GOES satellite is useful in monitoring cloud structure forced by these orographic effects. Satellite observations of the cloud-top region can reveal particle size and phase characteristics. If the cloud top region contains supercooled droplets, the near-infrared signature shown in the satellite image data can aid in identifying the glaciation process (Wetzel, 1995), which indicates the availability of ice crystals for efficient snow growth. By combining satellite remote sensing information on the structure and evolution of the cloud system with kinematic and thermodynamic data from observations and mesoscale model output, the forecasting process can incorporate analysis techniques specific to orographic scenarios.

This paper presents techniques that can be used to improve the accuracy of quantitative snowfall forecasting and analysis in mountainous regions. Data from a research program on winter orographic precipitation processes provide the framework within which to demonstrate the value of adding auxiliary resources such as targeted sensor systems at high altitude sites, satellite remote sensing methods, creation of a local snowfall climatology, and mesoscale modeling with graphical products tailored to orographic forecasting. The added benefit of this approach is examined in case studies for a specific mountain range in the northern Colorado Rocky Mountains.

2. Field Study Overview

This research uses case studies of well-documented snowfall events over a north-south oriented mountain ridge to evaluate the effects on snowfall production due to mesoscale dynamics, mixed-phase cloud microphysics and thermodynamic profiles over orographic terrain, and to demonstrate procedures designed to improve short-term forecasting of snowfall in this environment.. The study was based at the Desert Research Institute's Storm Peak Laboratory (SPL) (Figure 1), located in the Park Range near Steamboat Springs in northwest Colorado. This high-elevation (3220 m MSL; typically ~700 hPa pressure level) research lab has been used for

over 20 years to conduct basic research on cloud physics, cloud-aerosol interactions and alpine radiation climatology (Borys and Wetzel, 1997; Borys *et al.*, 2000; Lowenthal *et al*., 2002).

The study was conducted in tandem with ongoing research related to the microphysical processes which determine snowfall production in orographic cloud systems. Research described here included the deployment of a high-resolution vertically-profiling radar (Figure 2) from the National Center for Atmospheric Research (NCAR), local rawinsonde soundings, meteorological mesonet data collection, ridge-top cloud and precipitation microphysical measurements, snow core sampling at multiple elevations, and numerical model simulations to evaluate snow accumulation forecasts for a 3-km resolution mesoscale grid centered over the mountain range. Data collection was conducted January-March 2001 and 2002 as well as December 2002.

In the series of in situ microphysical measurements at SPL, cloud droplet size distributions were measured using an aspirated Droplet Measurement Technologies (DMT) SPP-100 forward scattering spectrometer probe. Ice crystal size distributions, ice water contents and two-dimensional images were sampled using a Particle Measurement Systems 2DP optical array probe. These two microphysics instruments were mounted on a large vane which orients the sample inlet to the oncoming airflow. Computer control of the sample data provided 10-second instantaneous values plus 6-minute averages and integrated sample statistics for number, area and volume size distributions, liquid water content, mean and modal droplet sizes, and other parameters. Ice crystal habit, dimensions and masses were also obtained from the DRI Snow Video Spectrometer system (Borys et al., 2000). Cloud sieves were used to sample the volume concentration and mass flux of supercooled liquid water in cloud, and flow-oriented bag samplers provided measurements of precipitation mass flux. A high-precision OHAUS mass gage fitted with a large collection pan and located within a snow collection wind shelter was used to measure time series of snowfall mass accumulation at one-minute intervals. A continuously recording meteorological tower system provided 5-minute average and 10-second maximum values of variables such as wind speed and direction, air temperature, relative humidity, solar radiation, ozone, aerosol concentration, and additional atmospheric conditions. These data contributed to the analysis of cloud and precipitation events.

A transect of snowfall measurement sites was established along an east-west track, beginning west of Steamboat Springs on the Yampa Valley floor, approximately 10 km from the

base of the mountain range, and continuing with four sites of increasing elevation from the radar site (RDR) at the base of the mountain, at intervals of 400 m to the ski area Patrol Headquarters (PHQ) along the mountain ridge (approximately centered within Figure 2). Measurements were made of the following parameters in the core of new snow accumulated on snow boards: new snow depth (cm), average density (kg/m^3), total SWE (mm), temperature (^{o}C), crystal type (classification based on Magono and Lee, 1966), crystal size (mm), degree of crystal riming, and profiles of new snow layer density (g/m^3) in 2cm-depth layer intervals.

New snow depth from each precipitation event was measured as a total accumulation on a snowboard. The snowboard used was a 60 cm by 60 cm square and was cleared after each measurement. Snowboard core density was measured using a Snowmetrics T1 tube sampler and a hanging scale. New snow layer density was measured using a 66.6 cc stainless cutter and an Acculab VI- 4kg digital flat scale. Other observations included snow layer temperature, air temperature, wind and snow occurrence at the sample time. The sites were selected with some surrounding vegetation where possible to reduce the effects of wind on snowpack modification, but were located within sufficient clearing space to minimize undercapture. When possible, the data collection sites were located near established meteorological data collection sites. Snow sampling was conducted on a storm event basis during 16 January – 25 February 2002. A majority of the measurements took place while the snow event was still occurring, which reduced the effects of snowpack metamorphosis, and the comparative analysis with model forecasts was carried out on the snowfall accumulation up to that point in time (rather than the "total" snowfall for a given event).

A mesonet of surface meteorological reporting stations is operated continuously by the Steamboat Ski and Resort Corporation (SSRC) on the western face of the mountain ridge to support their snowmaking activities. This mesonet provided hourly time series measurements of temperature and relative humidity. SSRC operates an acoustic sensor along the ridge at PHQ and this was used to monitor physical snow depth, which was very useful in establishing the time sequence of snowfall accumulation. The acoustic sensor also provides a record of snow depth loss due to snowpack metamorphosis. DRI operates an anti-freeze tipping bucket precipitation gage co-located with the acoustic snow sensor. This was also the highest-elevation site of the snow measurement transect (PHQ).

The Multiple Antenna Profiler Radar(MAPR) is an advanced wind profiling radar developed by the NCAR Atmospheric Technology Division (ATD) to make rapid wind measurements in the lower troposphere. Instrument design is based on a 915-MHz wind profiling radar which has been modified to use the spaced antenna wind measurement technique (Cohn et al., 2001). The system has one transmitter and four vertically-pointing antenna sub-arrays for reception. The motion of the reflected signal across the array is tracked to calculate wind velocity. Output parameters include horizontal wind, Doppler (radial) velocity, volume reflectivity and velocity variance. Time frequency is typically 60 seconds and vertical resolution modes are 50-200 m. The MAPR was operated at the RDR site, a valley elevation on the western edge of the Park Range, during mid-January to early March 2002. The ATD GPS-Loran Atmospheric Sounding System (GLASS) provided balloon profile data during event periods, and surface meteorological measurements (pressure, temperature, wind, humidity, radiation, precipitation) were conducted at the radar continuously during the study period.

The Regional Atmospheric Modeling System (RAMS) model (Cotton et al., 2003) Version 4.29 developed at Colorado State University (CSU) was run by CSU in a nested configuration similar to that described by Meyers *et al.* (2001). The model for the present simulations contained an outer domain at 48 km resolution, and two inner domains at 12 and 3 km (Figure 3) horizontal grid resolution, respectively. The terrain-following sigma-z vertical coordinate system had 36 levels, with grid spacing stretching from <150 m near the surface to approximately 1000m at and above 9 km. The model used the single-moment, mixed-phased microphysical scheme described by Walko *et al.* (1995), with prognostic fields for cloud droplets, rain, pristine ice crystals, snow, aggregates, graupel and hail (Meyers *et al.*, 1992a,b). Hydrometeor sizes were distributed according to a gamma function. This model has been successfully used to simulate strongly forced conditions with high snowfall in the Colorado Rocky Mountains (Poulos *et al*., 2002).

3. Forecasting Tools for Mountainous Terrain

Methods for improving snowfall forecasts in radar-limited mountainous terrain are demonstrated and include: identification of key meteorological elements for common event scenarios, use of mesoscale model accuracy in predicting the evolution of these events (even when radar data continues to indicate no precipitation during the event), knowledge of local

snowfall climatology, incorporation of improved observational data from precipitation sensor and other meteorological instrumentation at high elevation sites, and application of satellite data to short-term forecasting and trend analysis.

An empirical relationship commonly used to estimate snow depth from model-predicted precipitation water flux is the observed decrease in snow density as ambient air temperature decreases. A local climatology for winter snowfall density was created for use in the Park Range. Figure 4 presents a time series of snow depth accumulations measured at multiple elevations during January and February 2002 and Figure 5 depicts the snow densities for these samples. The measurements from individual storm events and the period-average values shown at the right end of the chart indicate that most event densities and average snow densities were quite low, with characteristics of greater densities at the lower elevations and increasing density with progression of the season from mid-winter. The elevational and seasonal tendencies are likely associated with the temperature dependence and mixed-phase growth mechanisms observed in these orographic systems. Measurements made earlier in the season might be expected to show a decrease in snow density from late fall toward mid-winter due to air mass characteristics.

A comparison of air temperature and new snow density for the three highest elevation sampling sites during snow events in January, February and December 2002 is shown in Figure 6. Air temperatures during the period of maximum snow accumulation along the ridge-top were obtained from the meteorological tower data obtained from the SSRC meteorological network and sensors at PHQ and SPL. For comparison, also shown in this figure are the data values from a table often used in NWS operations (NOAA, 1997) to estimate new snow density from local air temperature. A second method used by forecasters is the "10 to 1" rule (e.g. density of falling snow always assumed to be 10%). The data shown in Figure 6 indicate that the 10:1 rule is not reliable in this locale and that the NWS Meltwater Conversion Table would underestimate the density of new snow. Correlation between the measured air temperature and new snow density explained 52% of the variance. Similar results were found in previous studies (Judson and Doesken, 2000). A linear fit to the data yields the following relationship: $D = 0.16 + 0.008\ T$, where T is the average air temperature during the major period of snowfall. This relationship was applied to case study analysis and QPF as discussed in Section 4.

Acoustic snow depth gages are available at an increasing number of mountain sites and are important sources of verification and short-term forecasting information. The SSRC operates an acoustic snow depth sensor at the Patrol Headquarters site (PHQ) on the ridge, and these data can be accessed by modem. The instruments are located in a clearing of trees to allow protection from wind bias. An antifreeze-type recording tipping bucket precipitation gage is operated next to the acoustic sensor. Time series of measurements from these two instruments (Figure 7) is extremely valuable in determining the SWE and physical snow depth accumulation rates at high elevation (3170 m MSL at this site) for testing the validity of model parameters. The RAMS model used for this research has been modified to produce realtime graphics of predicted time series of snow accumulation at specific grid points, and the grid point locations have been tailored to match available measurement locations. The simultaneous snow depth and snow water time series also permit concurrent analysis of new snow density (Figure 8). These density estimates are very close to measurements taken manually by the snow survey samples obtained at the same location. All measurements of density were <0.09 except for a high-density period on the morning of Day 352, and manual sampling on that morning indicated density of 0.135 in the upper 8 cm of the accumulated snow. This snow event provided very rapid accumulation, which can create errors in gage measurements due to snow piling up on the gage perimeter and then falling into the gage en masse.

One of the most valuable methods of improving short-term weather prediction in mountainous terrain is to more fully incorporate point data such as the snowfall and snow density observations into the interpretation of the current and past few hours of meteorological events, with comparison to and updated interpretation of the available mesoscale model output. While the Park Range suffers from restricted radar coverage, it has the advantage of multiple measurement locations including SNOTEL sites, a ski area with modem-accessible acoustic snow depth gage and other observations, and the DRI Storm Peak Laboratory with web-accessible meteorological time series. This instrumentation and data access allow point validation of mesoscale model forecasts and evaluation of model performance that can aid interpretation of the ongoing event as well as provide the forecaster with improved composite knowledge of model biases under different event scenarios.

Ongoing advancement of local forecasting in mountainous areas can take advantage of improved model resolution that more fully resolves complex terrain. As each model

improvement is made, however, a new learning curve is imposed on the forecasters and previous model biases may be mistakenly accommodated and new biases combine to increase forecast error. It is therefore important to carry out case studies of snowfall events that represent characteristic types of synoptic evolution in the locale. This study uses three typical orographic snowfall events for the purpose of evaluating model performance and implementing additional forecast tools such as use of snow density-air temperature relationships, satellite data analysis and increased use of surface measurements.

4. Implementation for Case Study Analysis

Individual event scenarios are presented to demonstrate methods for improving the diagnosis and short-term prediction of snowfall accumulation when radar data are not available, using the tools described in Section 3. The results provide information on the overall performance of the RAMS 3-km grid mesoscale model in forecasting QPF in differing winter storm events, and focus on the discussion on methods for incorporating routinely available observations and operational model output to enhance snowfall forecasting and verification in mountainous areas.

4.1 Moist, sustained westerly upslope flow

This snowfall event made the headlines in regional news and created long lift lines on the local ski slopes, as a "powder day" for which the Steamboat ski resort is well known. While events of low density snow and associated rapid accumulation of snow depth are common during mid-winter in the Park Range, the ability to identify the intensity of these events is hampered by the lack of radar signal in the area. Key meteorological elements for this case study are sustained westerly flow and a combination of moisture and temperature profiles that optimize the Bergeron-Findeisen process for crystal growth.

A positively-tilted trough extended across the western United States as indicated by the 500-hPa height analysis at 0000 UTC 16 January (Figure 9). A series of weak short waves in association with the trough moved across northern Colorado during the morning hours of 16 January. Model cross-sections from 0000 UTC 16 January Eta model run for Steamboat Springs indicated weak instability through 0600 UTC 16 January. A shallow layer of moisture was available with 80% relatively humidity up to 600 hPa and with west flow (15 kts) at 700 hPa. The upper level water vapor and cloud top temperature distributions obtained from satellite

imagery indicated a large area of sub-tropical moisture advecting across the southwestern portion of the United States. A 50+ m s^{-1} (120 kts) jet at 300hPa sustained the moisture feed ahead of the trough. With modest precipitation amounts expected with this event, the Grand Junction Weather Forecast Office (GJT-WFO) forecasted snowfall amounts of 1 to 2 inches over lower elevations around the town of Steamboat Springs with 3 to 6 inches over higher elevations in the Park Range.

The shortwave dynamic forcing and significant upslope flow in a fairly moist regime generated a large elevational gradient of snowfall amounts across the Park Range by 1200 UTC 16 January. Snow amounts increased markedly from the town of Steamboat Springs which received only 2 cm snowfall to the ridge-top location where 32 cm accumulated snowfall was measured, which exceeded GJT-WFO forecasted snowfall amounts for the Park Range. The RAMS predicted maximum precipitation rates (1.5-2.5 mm/hr) in the central Park Range to occur in a narrow time window centered on 04 UTC; see (Figure 10). Precipitation gage measurements at the radar site also show the primary pulses of snowfall in the central portion of the Park Range to occur during 0200-0600 UTC. Figure 11 is a time series of data parameters obtained from the MAPR radar located near the base of the Park Range near Steamboat Springs. The radar reflectivity signal-to-noise ratio profiles represent the intensity of precipitation through the echo region with most intense precipitation during 0200-0500 UTC. The reflectivity increases beginning 0000 UTC on 16 January, diminishes at 0600 UTC and tapers off to background echo signal levels by 1400 UTC. The MAPR vertical velocities are indicative of snowfall rate, and horizontal wind profiles provide information on wind velocities and shear. A temporal change in airflow seen with MAPR was forecast well by the RAMS model, and was associated with a shift in the zone of maximum orographic precipitation from the northern Park Range early, to the central and southern portions of the range in later hours.

Figure 12 depicts a comparison of snow water equivalent (SWE) depths measured at five snow survey sites along an elevational transect extending from west of Steamboat Springs to the ridge-top, and QPF (accumulated SWE) predicted by the RAMS forecast model for those locations. Model values of SWE were bilinearly interpolated from four 3-km grid points surrounding each site location. The sampling transect points are spaced closely enough that they are sequentially separated by just one or two model grid points. The RAMS model predicts snowfall rate in terms of water-equivalent flux (rather than snow depth accumulation rate), so

SWE values are compared. The accumulation period and ending time for the model output was selected to match the snow sampling time at each site. In this case, the verification periods for the SWE total accumulation were 22.0 to 29.5 hours (depending on sample site location) after the model initialization at 1200 UTC on 15 January.

The SWE forecast matched that of the observation (10 mm) at the highest elevation sampling location, but the model under-predicted SWE at the lower elevations. If the temperature-density relationship presented in Section 3 had been used at the forecast time, the predicted snowfall accumulations for the higher elevation zone of the Park Range would have been large enough to issue a winter storm warning. However, the RAMS model also predicted temperatures in the sub-cloud and lower cloud layer approximately 5^{o}C warmer than observed by rawinsonde and surface measurements, which may have been caused by inadequate simulation of the moist adiabatic processes during forced orographic ascent. The model topography smoothed to a 3 km grid creates ridge-top surface elevations in the model that are on the order of 500 m lower than the actual envelope of the mountain range. A method to more adequately simulate orographically forced cloud processes is to use a "silhouette" topography which applies the maximum elevation data available (from the 30-sec data in this case) to all model grid cells where elevations occur over a certain value (such as 3 km). The RAMS model also allows for output of sounding profiles at any gridpoint in the simulation, and these can be used to evaluate the characteristics of parcels lifted from upwind of the mountain range due to topographic forcing.

A number of other aspects of the RAMS model forecast accuracy can be demonstrated using the available measurement data. Cloud base was estimated from the GLASS profiles and the SSRC mesonet data to be ~ –5 ^{o}C and 2100 m MSL (significantly below the ridge-top level). This corresponds well to the RAMS forecast cloud water distribution shown in a 0600 UTC west-east cross-section. The limited temperature range of the cloud layer and the westerly flow profiles that promoted orographic uplift (Figure 13) in the central Park Range allowed very efficient diffusional snow growth. The model cross-section for 0400 UTC depicts uplift directly upwind of SPL at temperatures near –15 ^{o}C. Ice crystals observed at SPL during the early period of snowfall were broadly branched dendrites with light to moderate riming at concentrations < 10/liter, mixed with cloud droplets with average diameter 10 µm and number concentrations 580 cm^{-3}. While the temperature regime allowed efficient water evaporation of

droplets and diffusional growth of crystals via the Bergeron effect, the relatively high concentrations and small sizes of cloud droplets also indicate conditions where the availability of aerosol that reduces droplet-to-crystal collection efficiency and thus suppresses riming growth and snow density (Borys et al., 2003). As the snowfall period progressed, cloud water was consumed by the diffusion-dominated crystal growth process and the crystals were predominantly unrimed dendrites. Microphysical observations confirmed RAMS model forecasts that supercooled cloud water was no longer present over the mountain range after 0600 UTC.

Additional information on snow growth processes in orographic clouds can be obtained from satellite data analysis, including the use of quantitative parameters to characterize cloud microphysical structure and time-lapse animations to indicate cloud layer evolution (Wetzel, 1995). Deep ice cloud covered the study region in the early hours of the precipitation event, but during the period that produced very low density snow, the upper level cirrus had moved away from the area and local cloud tops were at mid-levels. Cloud top temperatures observed in the IR imagery were –20 to –23 ^{o}C during the period of maximum snowfall accumulation, corresponding to GLASS profiles from balloons launched at 0207 and 0420 UTC that indicated cloud top near –25 ^{o}C (5100 m MSL). Satellite digital image data were used to calculate the difference between equivalent cloud top temperatures in the GOES infrared (IR) and near-infrared (NIR; 3.9-μm channel) images. This T_{IR} -T_{NIR} brightness temperature difference (BTD) at night is generally negative for cloud that is primarily composed of ice crystals at cloud top and near zero or slightly positive for mixed-phase or water cloud (Baum *et al*., 1994). A time series of IR images and BTD data indicated that the deep cirrus shield moved south away from the study location at 0300 UTC, revealing a view of a mixed phase cloud beneath that became more glaciated with time (after 0600 UTC), and the cloud top subsequently warmed considerably after 1600 UTC and dissipated.

4.2 Southwest blocking and airflow decoupling

A broad positively-tilted trough extended over the western United States at 0000 UTC 29 January 2002 as denoted by the 500-hPa height analysis shown in Figure 14. Strong gradient southwest flow ahead of this system was situated over north-central Colorado with a 75 m s^{-1} (150 kts) jet core at 250 hPa by 0000 UTC 29 January. In addition, a slow-moving baroclinic

zone and associated surface cold front moved across northwest Colorado between 0000-1200 UTC 29 January. The environment ahead of the cold front was fairly unstable with a lifted index of -1 taken from the 0000 UTC 29 January sounding at GJT. Behind the cold front, the air mass was moist with relative humidity > 80% up to 550 hPa, and low level winds were predominantly westerly. At 700 hPa, temperatures fell from -8°C to -14°C between 0000-1200 UTC 29 January. This cold advection kept shallow instability over the northern Colorado mountains.

As the trough moved eastward from the California coast toward the desert southwest, shifting airflow slowed the movement of the thermal gradient over northwest Colorado. With winds parallel to the thermal gradient, several embedded vorticity maxima moved across the area enhancing the potential for significant snowfall. Southwest flow typically does not produce significant snowfall over the Park Range, primarily because it is located to the lee of the Flattops Plateau (~3600 m MSL) and a mountain "rain shadow" effect typically prevails. However, the strong slow-moving baroclinic zone and very strong winds aloft generated strong upward vertical motion which overcame the mountain shadow effect. The air mass stabilized over the Park Range after 0000 UTC 30 January. As a deformation axis developed over northern Colorado by 0600 UTC 30 January, light snow persisted across the region until trough passage occurred by 1200 UTC 31 January. In spite of the unfavorable flow regime for heavy snow for this region, the GJT-WFO issued a Winter Storm Warning for 1 to 2 feet at elevations above 9000 ft in the Park Range, with a snow advisory for 4 to 8 inches for areas in the vicinity of Steamboat Springs. Snow depth totals shown in Figure 4 indicate approximately 17 cm (7 inches) accumulation at the Patrol Headquarters site (PHQ; 3170 m) with greater amounts received on higher ridges to the north, and 8 cm (3 inches) at a valley sampling site.

For this case, the strength and moisture content of the airflow during this event was sufficient to produce snowfall in this southwesterly regime (Figure 15) but the flow became decoupled and convergence in the mid-mountain elevation zone (see wind profile near 1000 UTC in Figure 15) may have caused a slightly larger SWE capture below the ridge-top (Figure 16) and a wide distribution over the entire region (Figure 17). Although the RAMS did not reveal larger accumulation at mid-mountain elevations, the observed wide distribution of snow across the model domain at middle and lower elevations was evident in the model simulations.

The RAMS model forecast indicated relatively warm temperatures in the precipitation zone (Figure 18). Time series of measurements at SPL provide evidence that the model over-

predicted air temperature during the snow event as in the 16 January case. The magnitude of the cooling trend from 0000 – 1500 UTC for SPL was forecast to be 5°C rather than the 10°C cooling observed at the elevation of ridge-top. This would cause higher estimates of snow density and thus under-prediction of snow depth accumulations. A more accurate (colder) forecast air temperature at ridge-top would have led to decreased estimates of snow density and increased snow depth predictions. The timing of the model simulation temperature minimum (approximately 1500 UTC) did agree with observations, indicating accuracy in predicting dynamic evolution. The later portion of the snow event (near 1600 UTC) with airflow blocking and downward motion is evident in both the MAPR data (Figure 15) and the RAMS model forecast (Figure 19).

4.3 Wraparound northwest flow

An open wave trough was located over the central Rockies as indicated by the 500-hPa height analysis at 0000 UTC 9 February 2002 (Figure 20). Eta-model time-height cross section over Steamboat Springs indicated limited moisture with this system with relatively humidity of greater than 80% found below 600 hPa after 1500 UTC 9 February. This system was also characterized by strong northwest flow throughout the event with +30 kts at 700 hPa through 1800 UTC 9 February. This strong flow continued through 9 February as the system deepened over western Kansas generating increased northerly flow over the Park Range, with relatively cold temperatures on 9 February (~ -15°C temperatures at 700 hPa). Embedded weak short waves wrapping around the closed low over Kansas enhanced snowfall amounts during the daytime hours. At 0000 UTC 10 February the trough axis had passed east of the Steamboat Springs area and precipitation ended by 0200 UTC. With limited moisture, GJT-WFO issued a snow and blowing snow advisory for 4 to 8 inches of snow for the Park Range, with only light accumulations for the town of Steamboat Springs.

Deepening of the low to the east of the Park Range and strong NW flow provided orographic uplift and precipitation (Figure 21). As moisture increased during the evening hours, snow began to fall across the Steamboat Springs area, commencing at 0300 UTC 9 February and continuing to the following evening. The time period of primary snow accumulation occurred after 1200 UTC during NW flow at ridge-top level that was accompanied by strong and deep upward vertical velocities (Figure 22). The GJX WSR-88D reflectivity (Figure 23) shows no

precipitation occurring over the mountain locations around Steamboat Springs. A combination of distance from radar, beam blockage and shallow precipitation structure often seen in winter storms results in this lack of radar signature. Winds measured at SPL verified this airflow pattern (Figure 24) and also shows a termination of precipitation when winds at the barrier level attained an easterly component near 2300 UTC.

For the event as a whole, significant precipitation coverage over the Yampa Valley was forecast (Figure 25; Figure 26) and was verified. RAMS forecast accumulations in the upper zone of the Park Range were very similar to observed (Figure 27), but more snow fell into the valley than was forecast. As in the previous two cases, the forecast air temperatures were warmer than measured on the Park Range during the precipitation period, which may have influenced the microphysical processes being simulated in the model, and also would have caused an under-estimate of snow depth values estimated from SWE and temperature conditions. The GJT-WFO operational forecasts for snow depth (up to 8 in; 20 cm) were less than observed at the higher elevations (38 cm at PHQ site). These results suggest that improvements in the model forecast temperatures, and the use of real-time measurement sites at higher elevations to track observed temperature trends, could increase the accuracy of short-term predictions for snow density and snow depth.

5. Discussion and Conclusions

Radar detection of snowfall is limited in many mountainous regions, so the combined use of model forecasts and other available observations becomes essential to prediction and verification of precipitation distribution. This study demonstrates techniques to more fully apply observations and mesoscale models in analysis of orographic snowfall. Ridge-top predictions of snow accumulation and timing were evaluated for three winter events in the Park Range of NW Colorado. The precipitation distribution as forecast by the RAMS mesoscale model was very similar to observed snow water equivalent values near ridge-top, but there was a tendency for under-prediction at lower elevations. Most forecast models provide QPF parameters for snow in terms of water equivalent rather than snow depth due to the difficulties in estimating the density of snowfall. Therefore, accurate forecasts of snow water equivalent as well as a reasonably accurate method for estimating snow density are needed. Field measurements of

several snow events in the study region have been composited to obtain an empirical relationship between air temperature and snow density in the typical elevation zone of precipitation for this mountain ridge. This dataset is specific to the region and typical cloud structure on the Park Range and while not necessarily relevant to other locales, provides a useful tool for estimating snow density. This study also demonstrated a method for real-time monitoring of snow density using snow water and acoustic snow depth measurements at high temporal resolution, the use of satellite remote sensing to characterize cloud depth and microphysical conditions during the evolution of a winter cloud system, and the application of snow survey data to conduct case study analysis of elevational transects created from high-resolution forecast model grids.

The case study analyses indicated that the operational forecasts of snow depth accumulation could be improved through the use of SWE forecasts and temperature-density relationships, but that further investigation and improvement is needed for the model simulation of air temperature profiles. In particular, it was evident that the model over-estimated air temperature in the zone of mixed-phase precipitation growth, and that the use of a smoothed grid elevation dataset contributes to warm bias by under-representing orographic effects on moist adiabatic processes. A more realistic representation of surface topography is planned for future model applications to use the "silhouette" of the topography (the highest elevations within the 30-second elevation database for terrain above 3 km) to more adequately simulate orographic effects on moist adiabatic processes during forced ascent over the mountain range. Graphical products for model profiles sited along the topographic cross-section of the primary airflow can be used to adjust estimates of adiabatic cooling in parcels lifted across the mountain range.

In orographic cloud systems, snow growth is most likely to be maximized near cloud base along mountain slopes and ridges. Measurement sites can be established at these locales through targeted cooperative arrangements with volunteer observers, mountain-located resorts or state agencies. An example of data acquistion at a ski area is used in this study. Meteorological observing sites are also currently being established at several mountain pass locations in Colorado for use in air and highway transportation, and similar opportunities likely exist in other states. Real-time interpretation of mountain-sited observations, applied in conjunction with tailored products from mesoscale models and case study examples of orographic effects, will lead to improvements in the quantitative forecasting of snowfall distribution.

Acknowledgments. Support for this research was provided by the Cooperative Program for Operational Meteorology, Education and Training (COMET) under UCAR Grants S02-38657 and S00-19126), and by a National Science Foundation (NSF) grant to the Desert Research Institute (DRI) through grant ATM-0004265. The COMET funding is provided by a cooperative agreement between the National Oceanic and Atmospheric Administration (NOAA) and the University Corporation for Atmospheric Research (UCAR). The views expressed herein are those of the authors and do not necessarily reflect the views of NOAA, its sub-agencies, or UCAR. Participation by scientists from the National Center for Atmospheric Research (NCAR) was supported by the NSF grant to DRI. NCAR is operated by UCAR under sponsorship of NSF. The authors extend appreciation for manuscript review to Preston Leftwich, National Weather Service Central Region Headquarters. Many thanks to DRI engineers (Rick Purcell, Dan Wermers), NCAR engineers and scientists including Ned Chamberlain, Mike Susedik, Terry Hock, and the staff of the NWS Grand Junction Forecast Office. Logistical assistance from the Steamboat Ski and Resort Corporation is greatly appreciated. DRI is an equal opportunity service provider and employer and is a permittee of the Medicine-Bow and Routt National Forests.

REFERENCES

Baum, B.A., R.F. Arduini, B.A. Wielicki, P. Minnis and S.-C. Tsay, 1994: Multilevel cloud retrieval using multispectral HIRS and AVHRR data: Nighttime oceanic analysis. *J. Geophys. Res.*, **99**, 5499-5514.

Borys, R.D., and M.A. Wetzel, 1997: Storm Peak Laboratory: A research, teaching and service facility for the atmospheric sciences. *Bulletin, Amer. Meteorol. Soc.*, **78**, 2115-2123.

Borys, R.D., D.L. Lowenthal and D.L. Mitchell, 2000: The relationships among cloud microphysics, chemistry, and precipitation rate in cold mountain clouds. *Atmos. Environ.*, **34**, 2593-2602.

Borys, R.D., Lowenthal, D.H., Cohn, S.A., and Brown, W.O.J., 2003: Mountaintop and radar measurements of aerosol effects on snow growth and snowfall rate. *Geophys. Res. Lett.*, submitted December 30, 2002, in press.

Cohn, S.A., W.O.J. Brown, C.L. Martin, M.S. Susedik, G. Maclean and D. B. Parsons, 2001: Clear air boundary layer spaced antenna wind measurements with the Multiple Antenna Profiler (MAPR). *Annales Geophysicae*, **19**, 845-854.

Cotton, W.R., R.A. Pielke, Sr., R.L. Walko, G.E. Liston, C.J. Tremback, H. Jiang, R.L. McAnelly, J.Y. Harrington, M.E. Nicholls, G.G. Carrio, J.P. McFadden, 2003: RAMS 2001: Current status and future directions. *Meteor. Atmos Physics*, **82**, 5-29

Heggli, M.F., and R.A. Rauber, 1988: The characteristics and evolution of supercooled liquid water in wintertime storms over the Sierra Nevada: A summary of microwave radiometric measurements taken during the Sierra Cooperative Pilot Project. *J. Appl. Meteor.*, **27**, 989-1015.

Judson, A., and N. Doesken, 2000: Density of freshly fallen snow in the Central Rocky Mountains. *Bull., Amer. Meteor. Soc.*, **81**. 1577-1587.

Lowenthal, D.H., R.D. Borys and M.A. Wetzel, 2002: Aerosol distributions and cloud interactions at a mountaintop laboratory. *J. Geophys. Res*., 107 (D18), 4345, doi:10.1029/2001JD002046.

Magono, C., and C.W. Lee, 1966: Meteorological classification of natural snow crystals. *J. Fac. Sci.*, Hokkaido University, **7**, 321-362.

Meyers, Michael P., Paul J. DeMott, William R. Cotton, 1992: New Primary Ice-Nucleation Parameterizations in an Explicit Cloud Model. *J. Appl. Meteor.*, **31**, 708–721.

Meyers, Michael P., William R. Cotton, 1992: Evaluation of the Potential for Wintertime Quantitative Precipitation Forecasting over Mountainous Terrain with an Explicit Cloud Model. Part I: Two-Dimensional Sensitivity Experiments. *J. Appl. Meteor.*, **31**, 26–50.

Meyers, M.P, E.M. Page, R.L. McAnnelly and W.R. Cotton, 2001: Operational fire weather support through the use of a mesoscale forecast model. *Prepints, Ninth Conf. Mesoscale Processes*, Fort Lauderdale, FL, 234-235. Amer. Meteor. Soc., Boston, MA.

National Oceanic and Atmospheric Administration, National Weather Service Observing Handbook Number 7. Surface Observations, Part IV, Table 2-14, "New Snowfall to Estimated Meltwater Conversion Table". Department of Commerce, Washington DC, 440 pp., 1997.

Poulos, Gregory S., Douglas A. Wesley, John S. Snook, Michael P. Meyers, 2002: A Rocky Mountain Storm. Part I: The Blizzard—Kinematic Evolution and the Potential for High-Resolution Numerical Forecasting of Snowfall. *Wea. and Forecasting*, **17**, 955–970.

Reinking, R.F., J. B. Snider and J.L. Coen, 2000: Influences of storm-embedded orographic gravity waves on cloud liquid water and precipitation. *J. Appl. Meteor*., **39**, 733-759.

Roebber, P.J., S.L. Bruening, D.M. Schultz, and J.V. Cortinas, Jr., 2002: Improving snowfall forecasting by diagnosing snow density. *Wea. Forecasting*, in press.

Walko, R.L., W.R. Cotton, M.P. Meyers, and J.L. Harrington, 1995: New RAMS cloud microphysics parameterization. Part I: The single-moment scheme. *Atmos. Res.*, **38**, 29-62.

Wetzel, M.A., 1995: Simulation of radiances for future AVHRR platforms with the AVIRIS spectral radiometer. *Int. J. Remote Sensing*, **16**, 1167-1177.

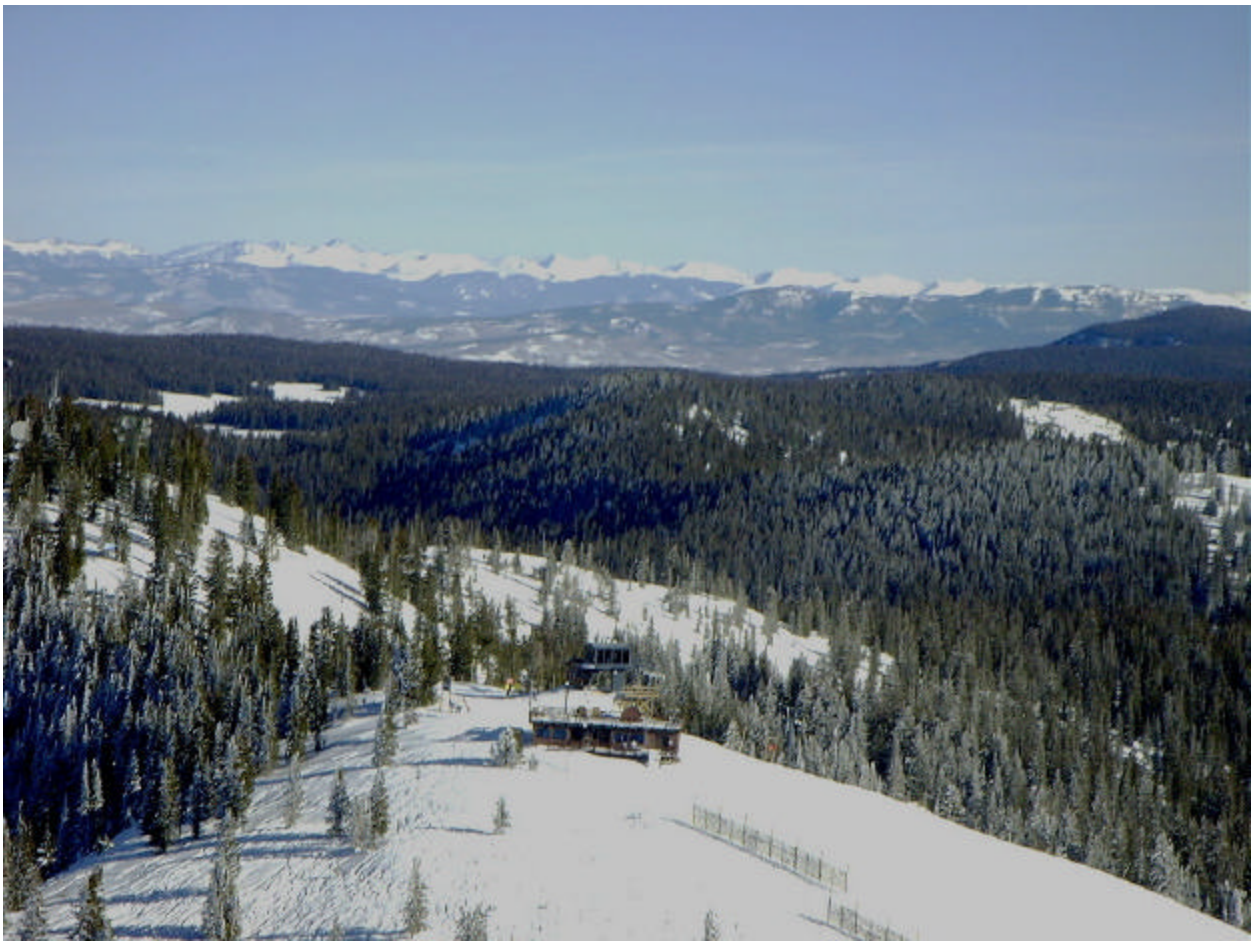

Fig. 1. DRI Storm Peak Laboratory at 3200 meters elevation along the ridge of the Park Range of northern Colorado.

Fig. 2. NCAR Multiple Antenna Profiling Radar (foreground) and Park Range (background).

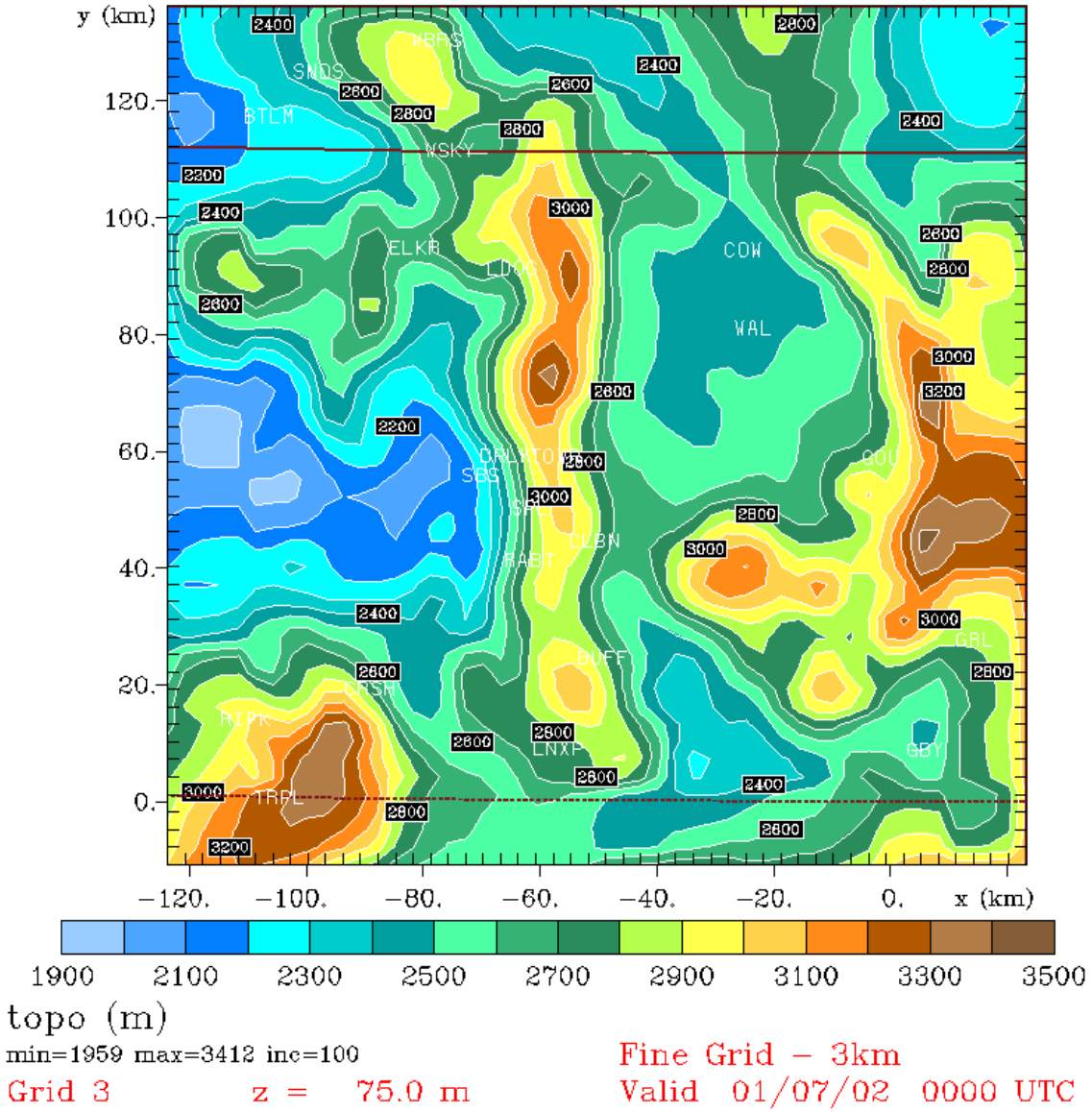

Fig. 3. Grid 3 topography for RAMS model. Snow sampling sites are near and immediately west of SPL, located at the 3000m contour marker in center of domain.

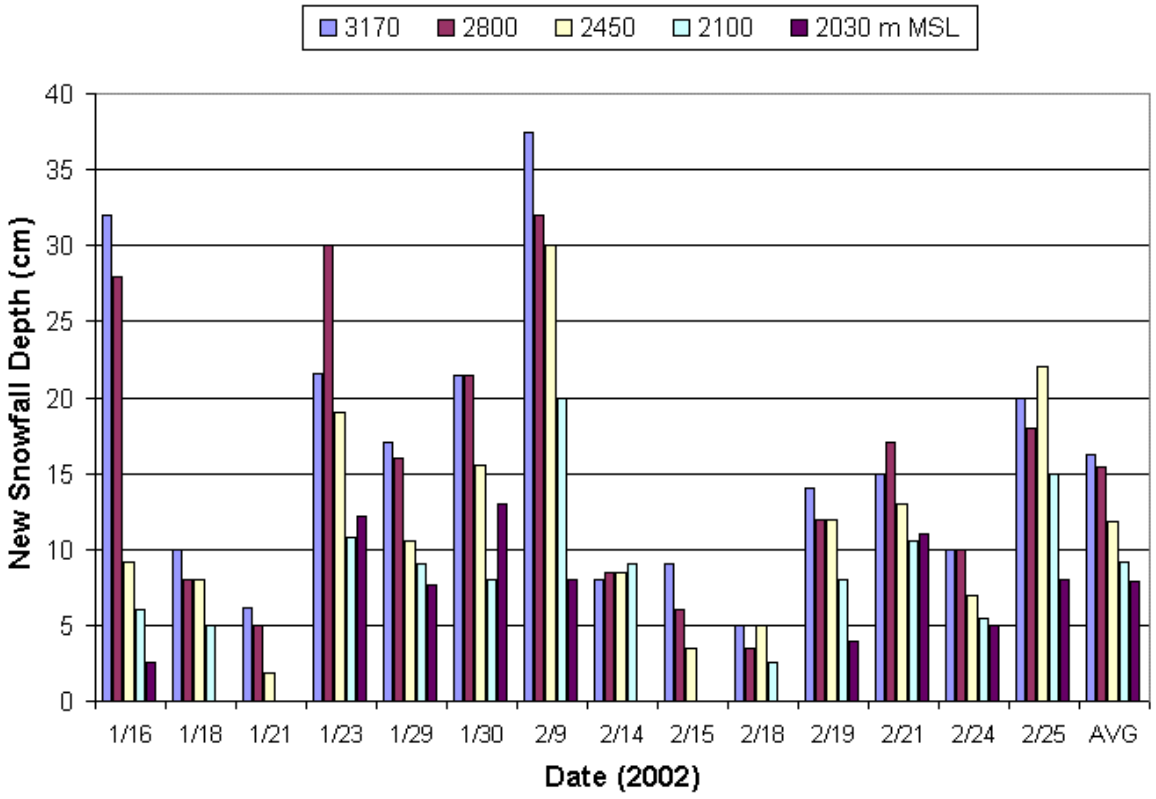

Fig. 4. Event time series of snow depth accumulation for sampling sites at elevations from 2030 to 3170 m MSL (6664 to10410 ft).

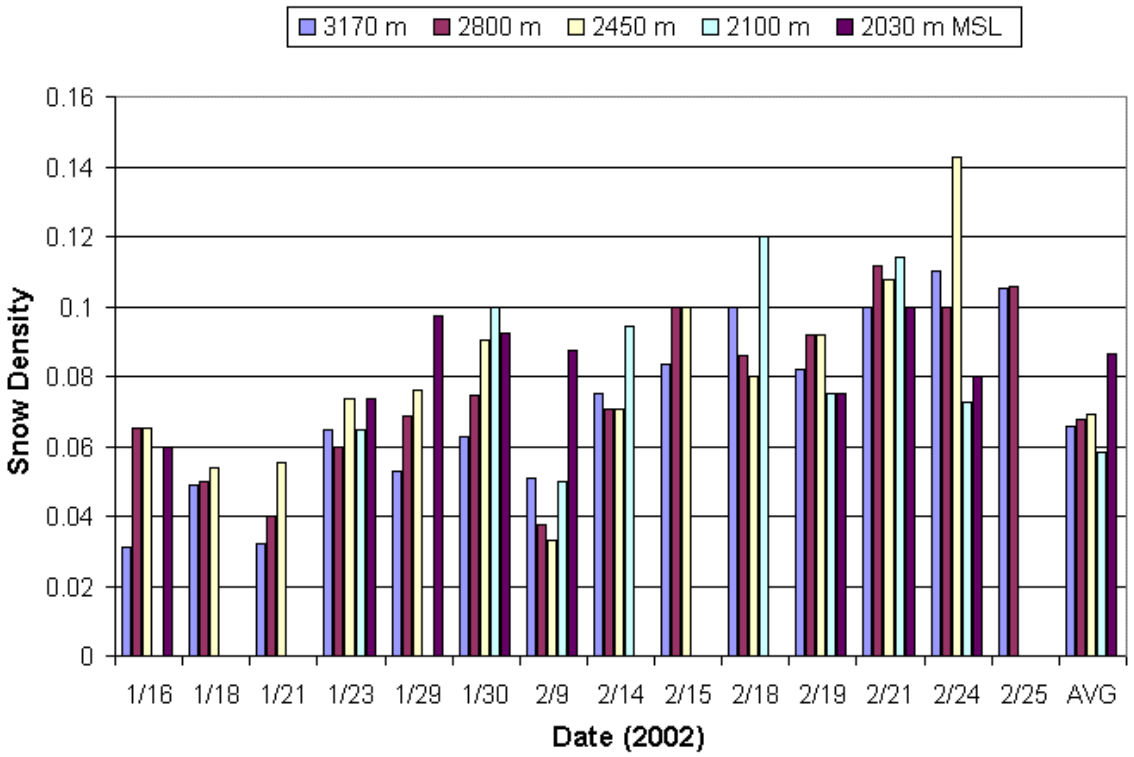

Fig. 5. Event time series of snow density for sampling sites at elevations from 2030 to 3170 m MSL (6664 to10410 ft).

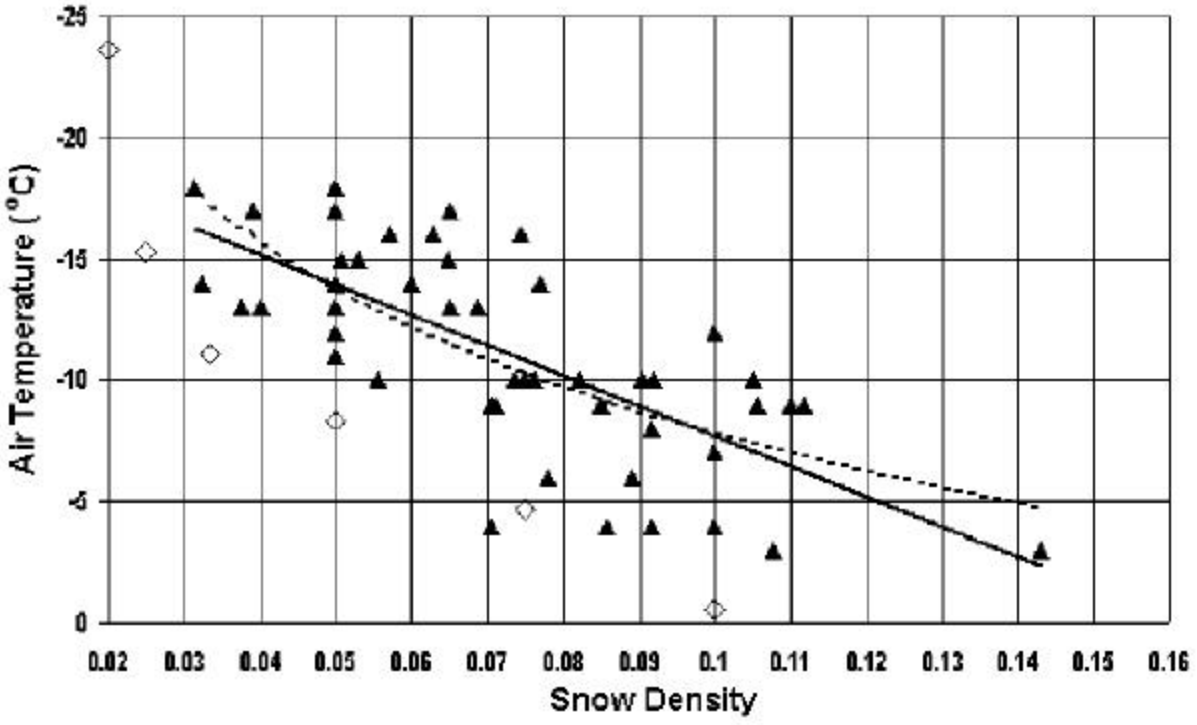

Fig. 6. Scatterplot showing the relationship between air temperature and new snow density (triangles) obtained from three sampling locations (at 2450, 2800 and 3170 MSL) in the Park Range during winter months of 2002; with linear curve fit (solid line) and exponential fit (dashed). Also shown are points obtained from the NWS New Snowfall to Estimated Meltwater Conversion Table (diamonds).

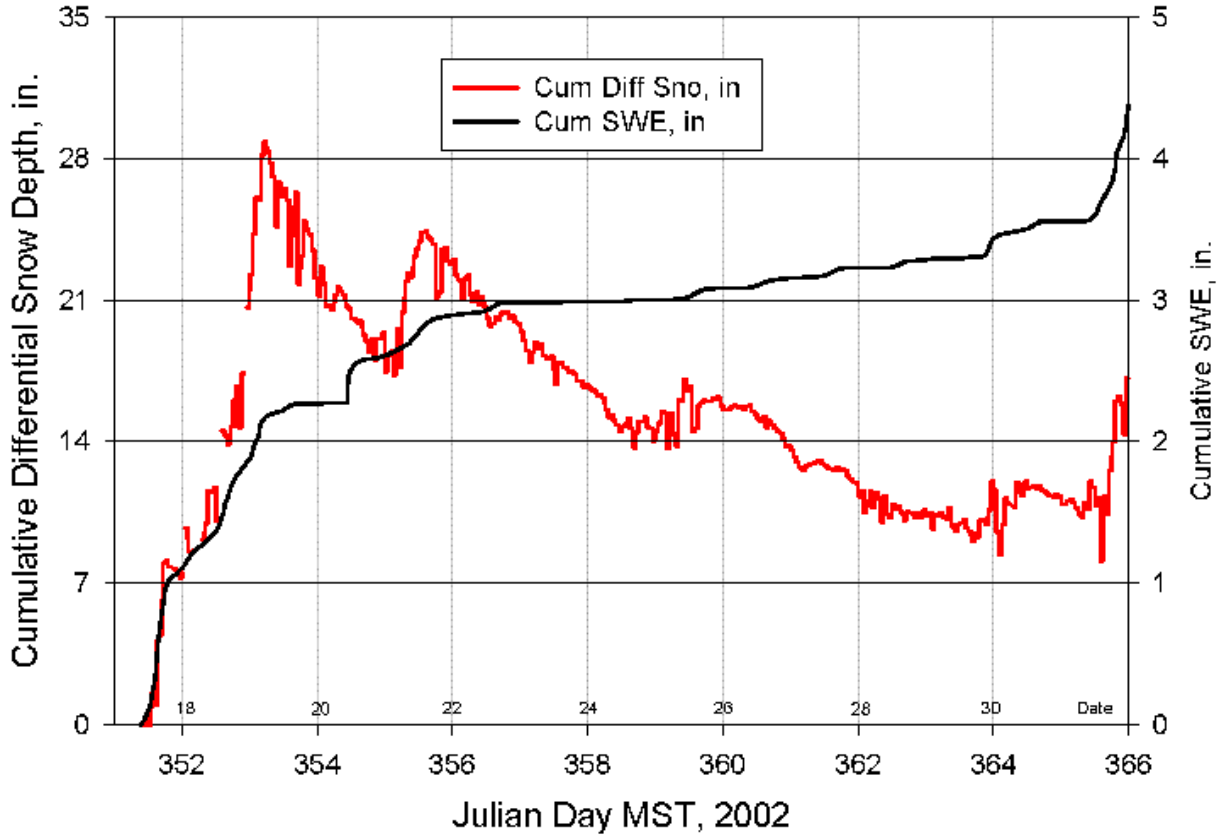

Figure 7. Time series of differential snow depth obtained from an acoustic snow sensor and cumulative snow water equivalent depth measured by an antifreeze tipping bucket gage at the Patrol Headquarters site for the last two weeks of December 2002. The differential snow depth increases during snow events, and then decreases between snow periods primarily due to snow settling.

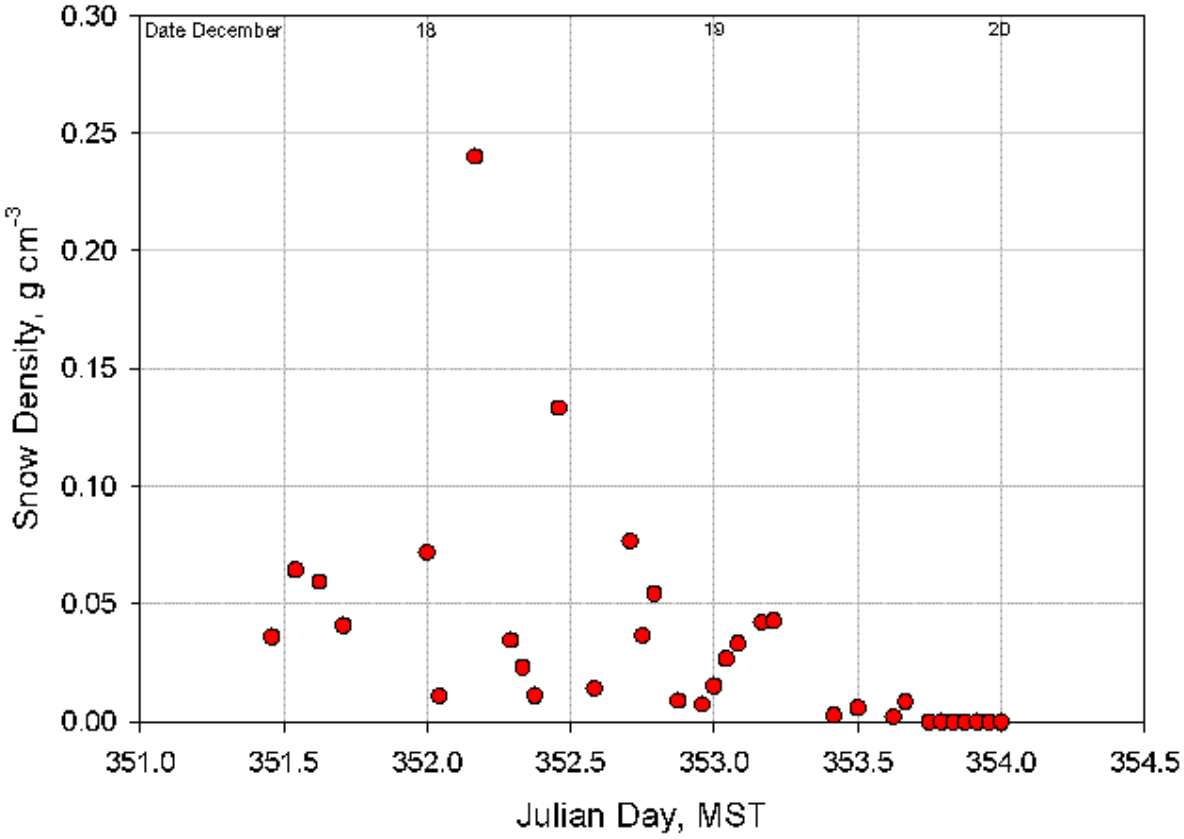

Figure 8. Time series of new snow density estimated for the first three days of the dataset shown in Figure 7.

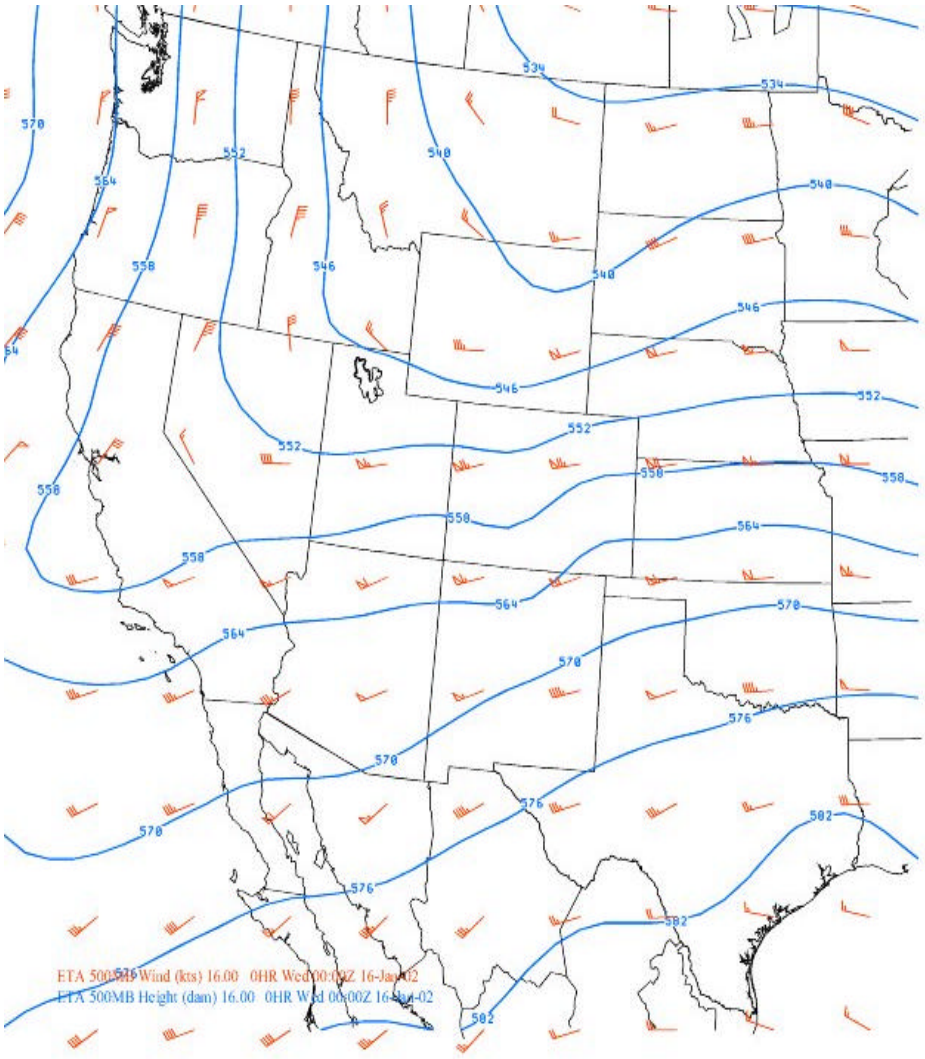

Fig. 9. ETA model 500 mb analysis of wind (kts; barbs) and height contours (dm) for 0000 UTC 16 January 2002.

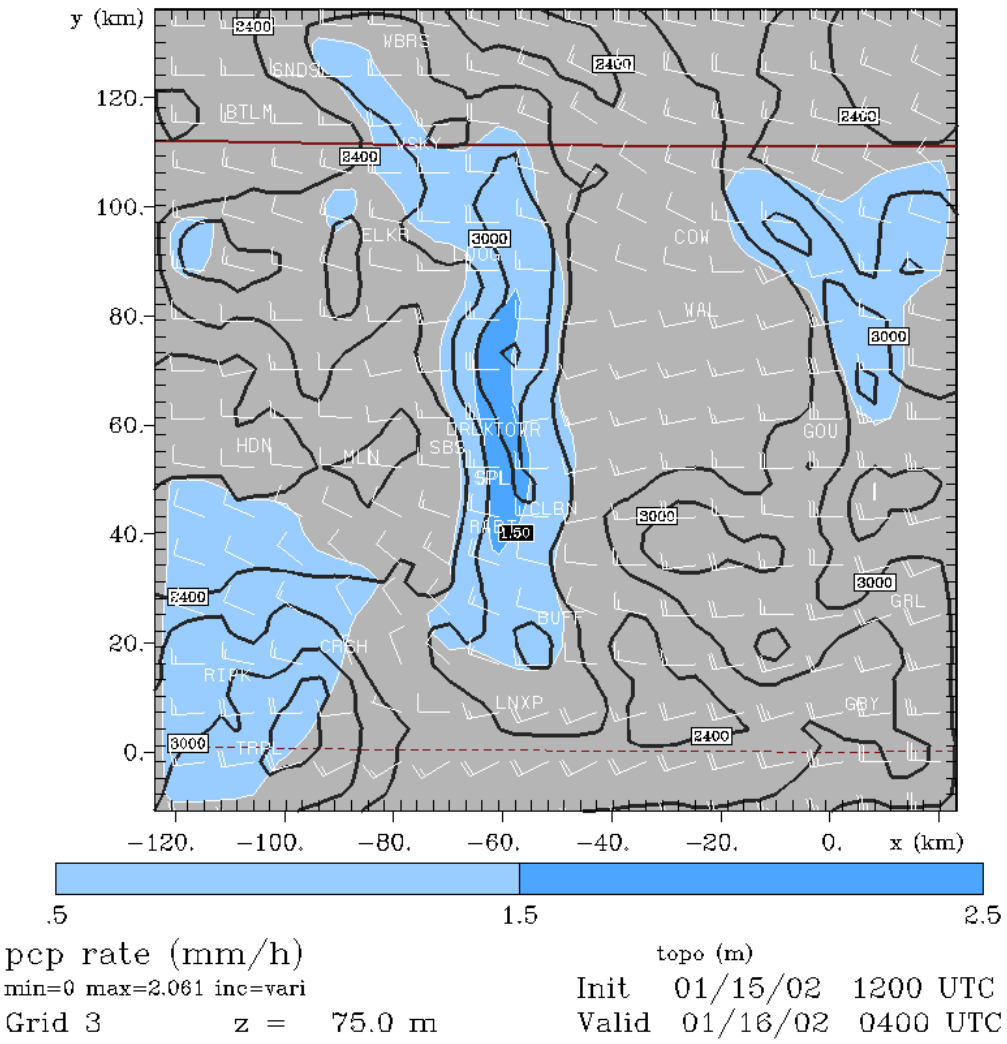

Fig. 10. RAMS model precipitation rate forecast at 04 UTC on 16 January 2002.

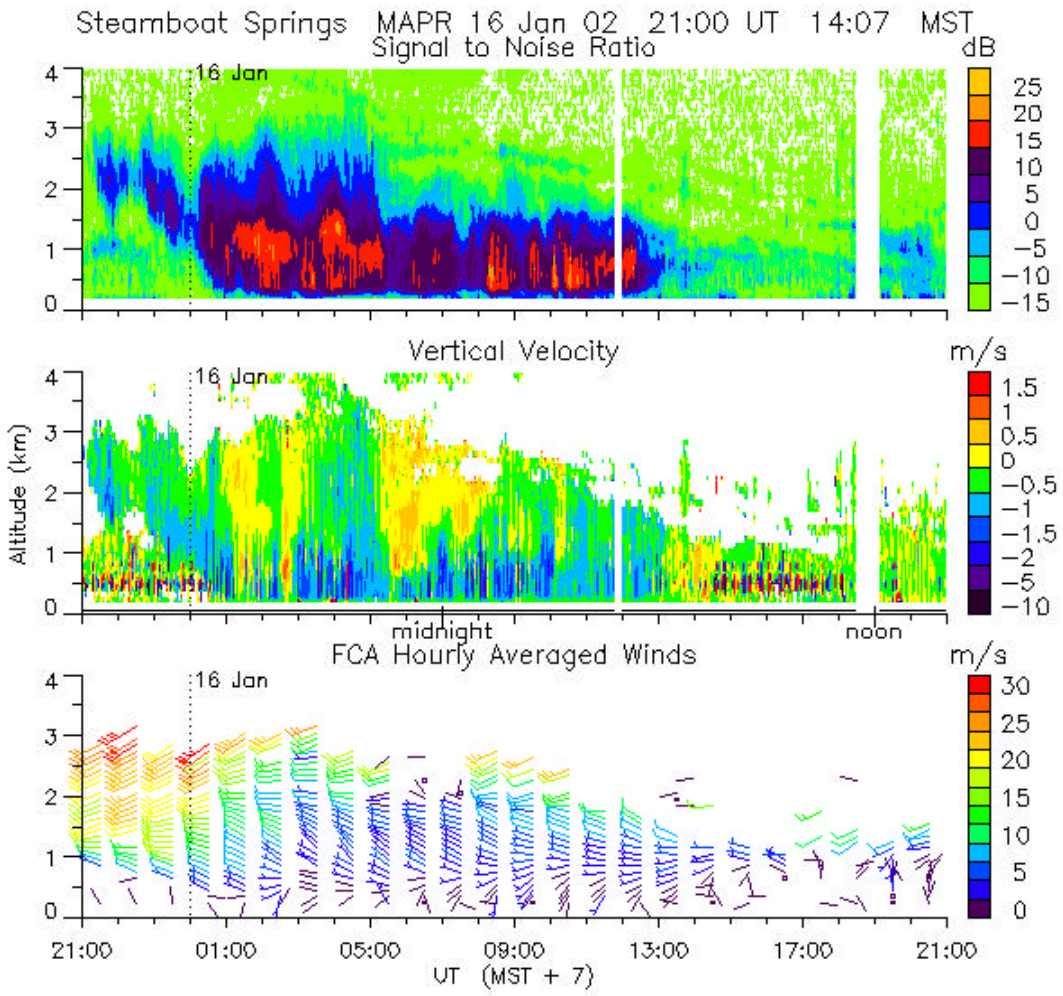

Fig. 11. NCAR MAPR radar profiles of reflectivity signal-to-noise ratio (SNR, related to precipitation intensity), vertical velocity (positive upward) and horizontal winds (upper, middle and lower panels, respectively) for 16 January 2002.

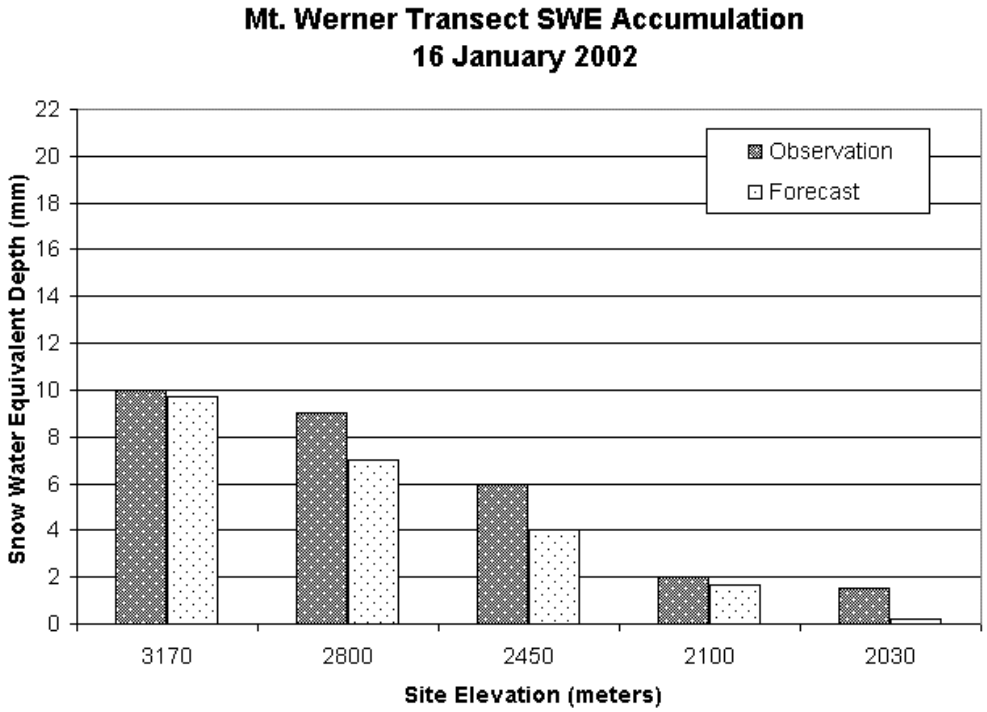

Fig. 12. Elevational comparison of observed and RAMS forecast snow water accumulations for 16 January 2002.

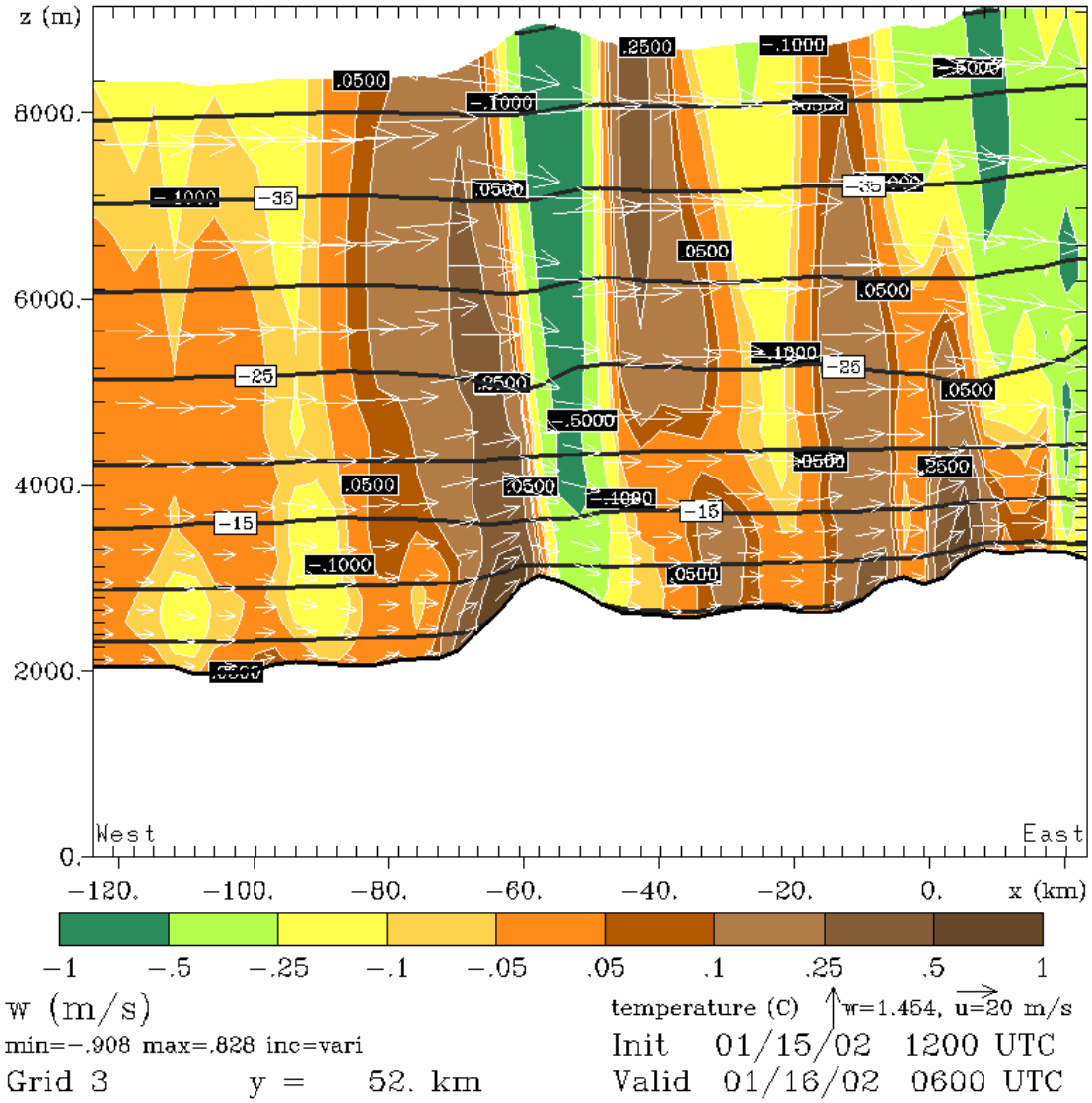

Fig. 13. RAMS model forecast west-east cross section of vertical velocity, temperature and air motion for 06 UTC on 16 January 2002.

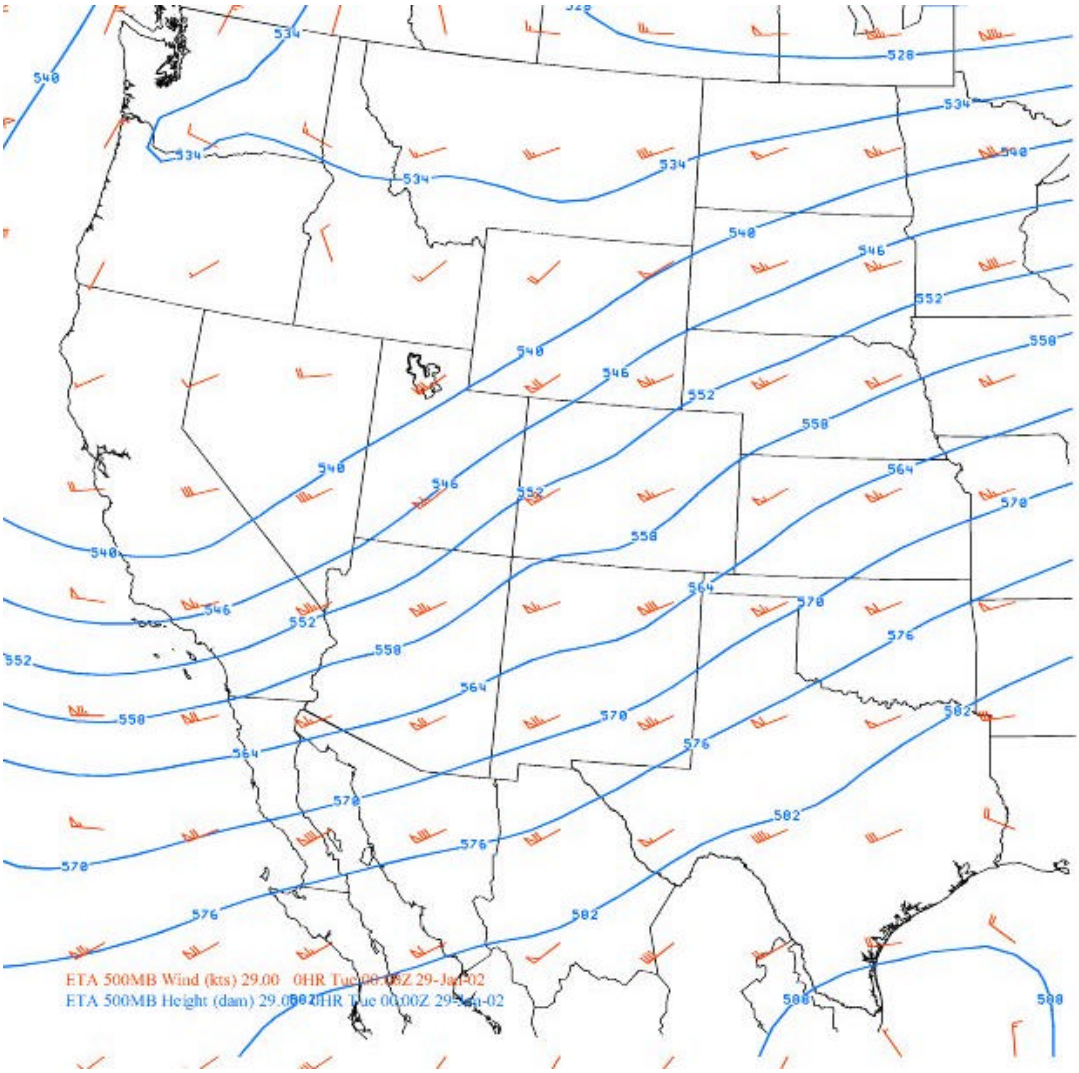

Fig. 14. ETA model 500 mb analysis of wind (kts; barbs) and height contours (dm) for 0000 UTC 29 January 2002.

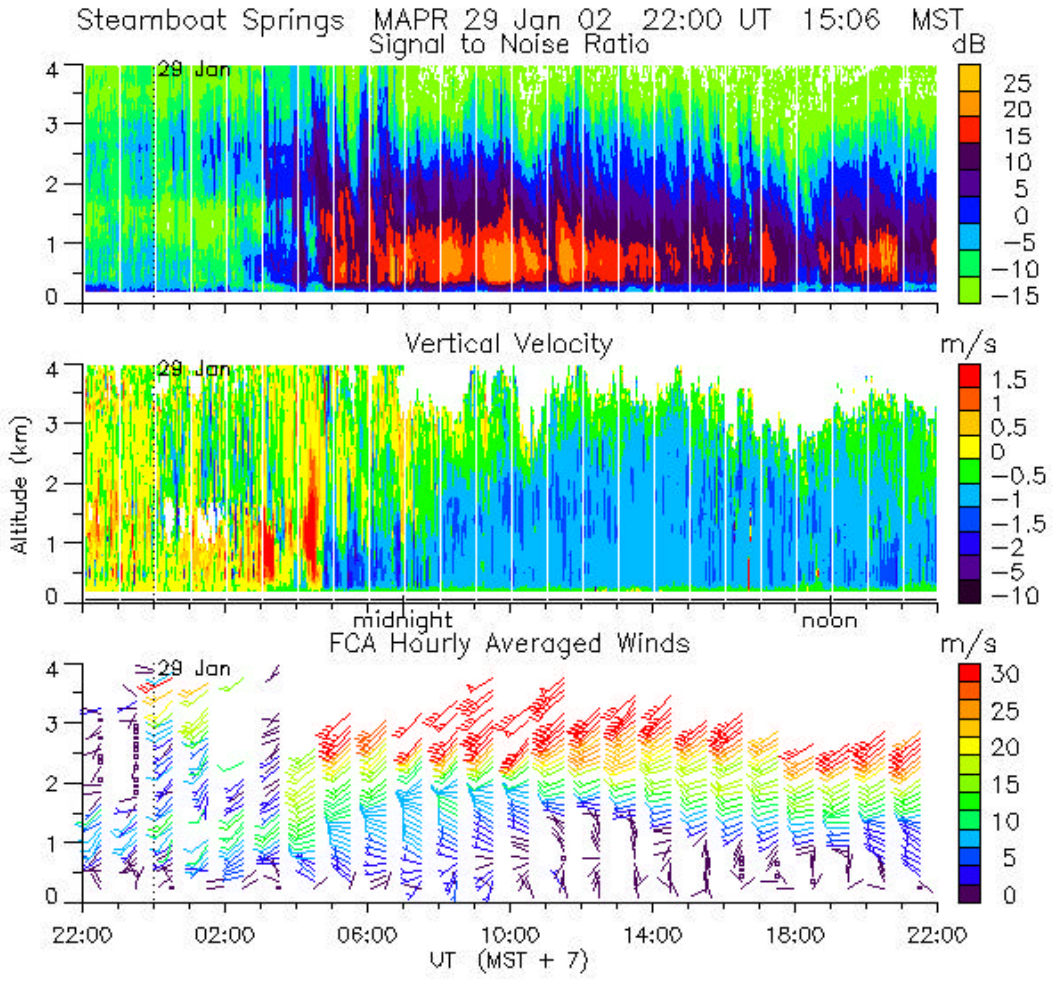

Fig. 15. NCAR MAPR radar profiles of reflectivity signal-to-noise ratio (SNR, related to precipitation intensity), vertical velocity (positive upward) and horizontal winds (upper, middle and lower panels, respectively) for 29 January 2002.

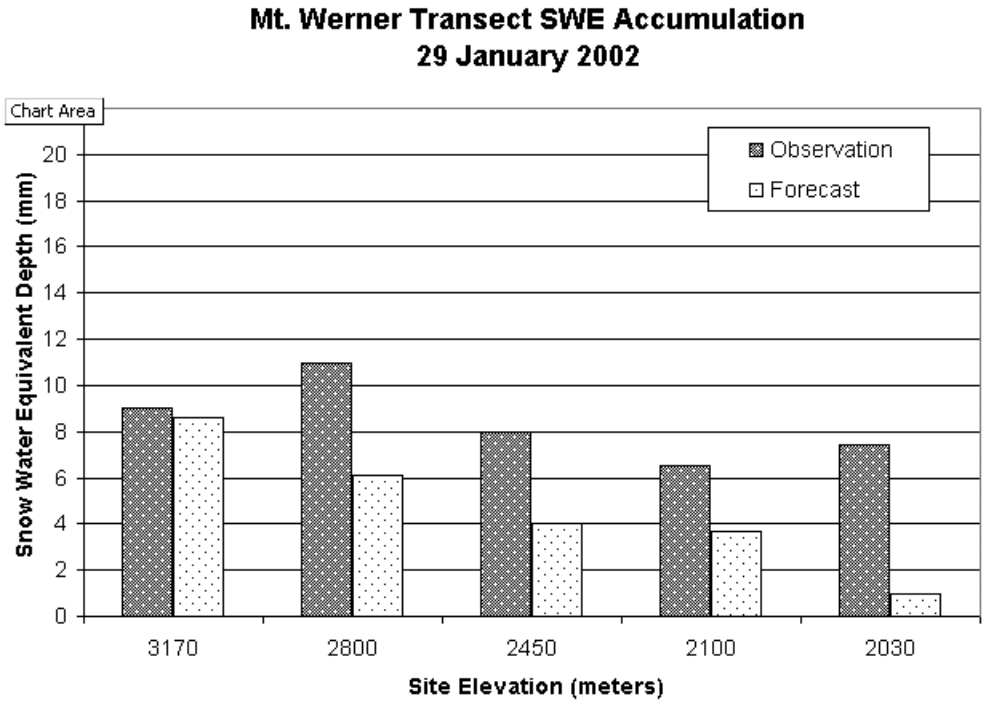

Fig. 16. Elevational comparison of observed and RAMS model forecast snow water accumulations for 29 January 2002.

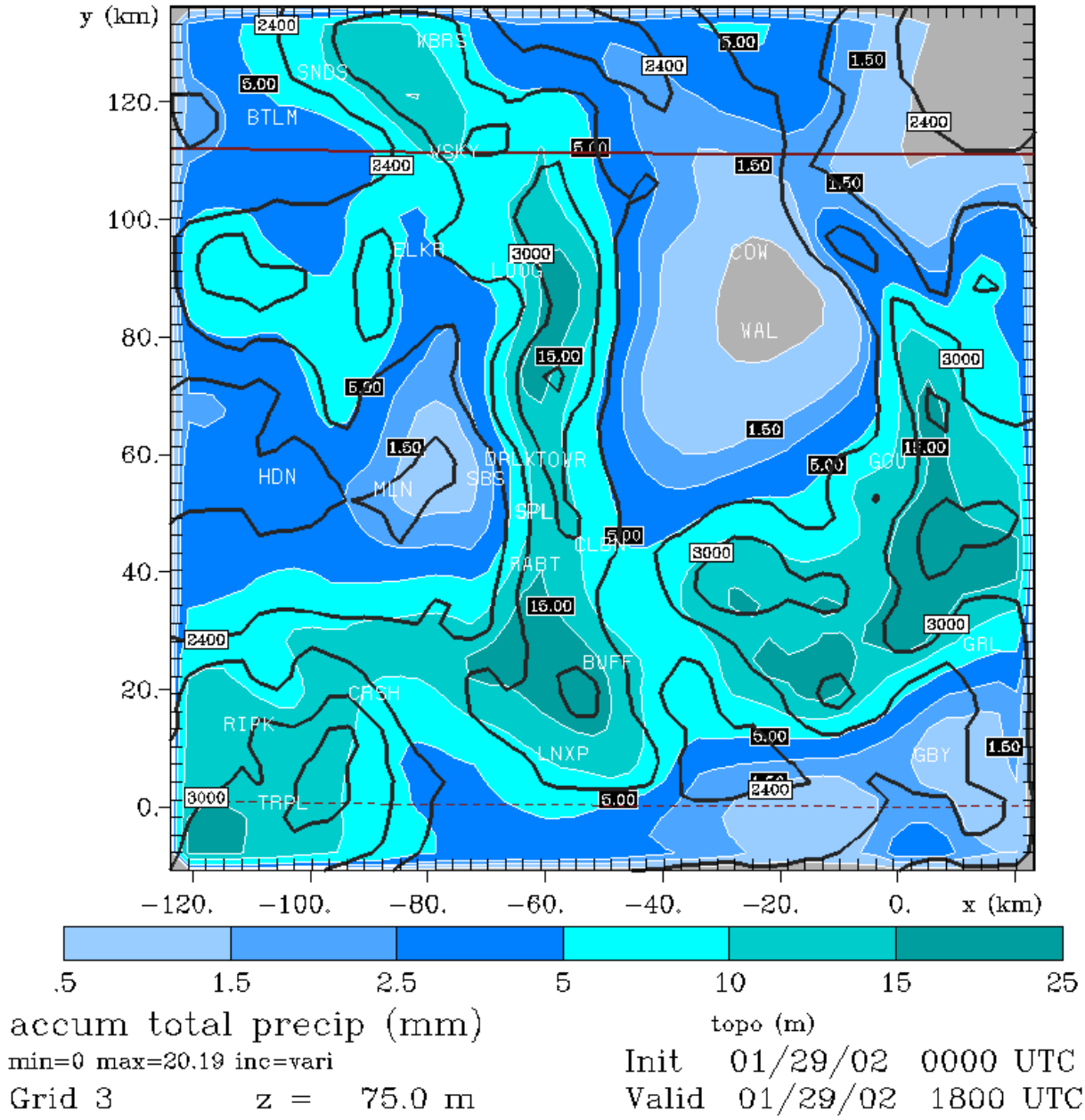

Fig. 17. RAMS model forecast of accumulated precipitation for the period 00 UTC to18 UTC on 29 January 2002.

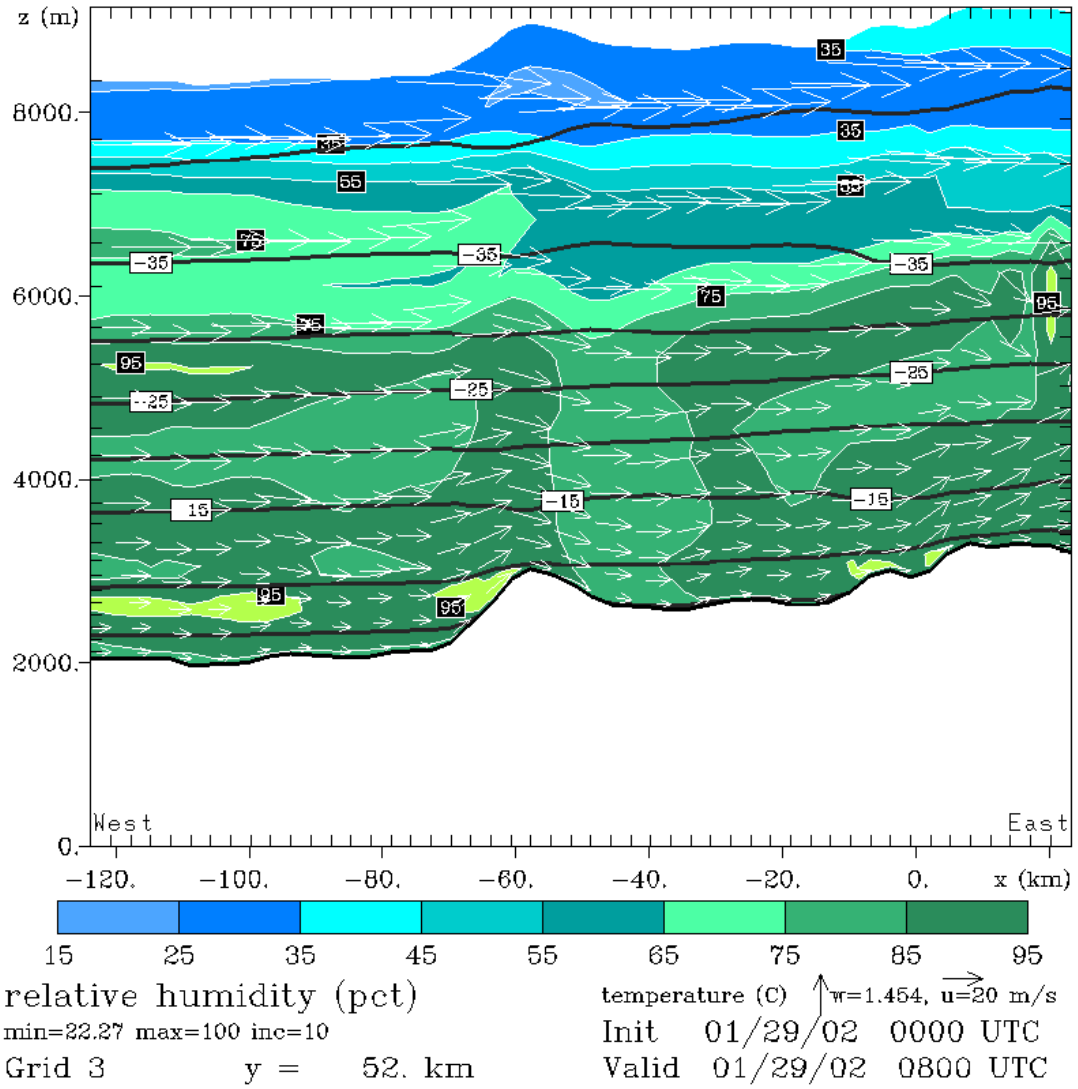

Fig. 18. RAMS model-predicted cross-section of relative humidity, temperature and winds for 08 UTC on 29 January 2002.

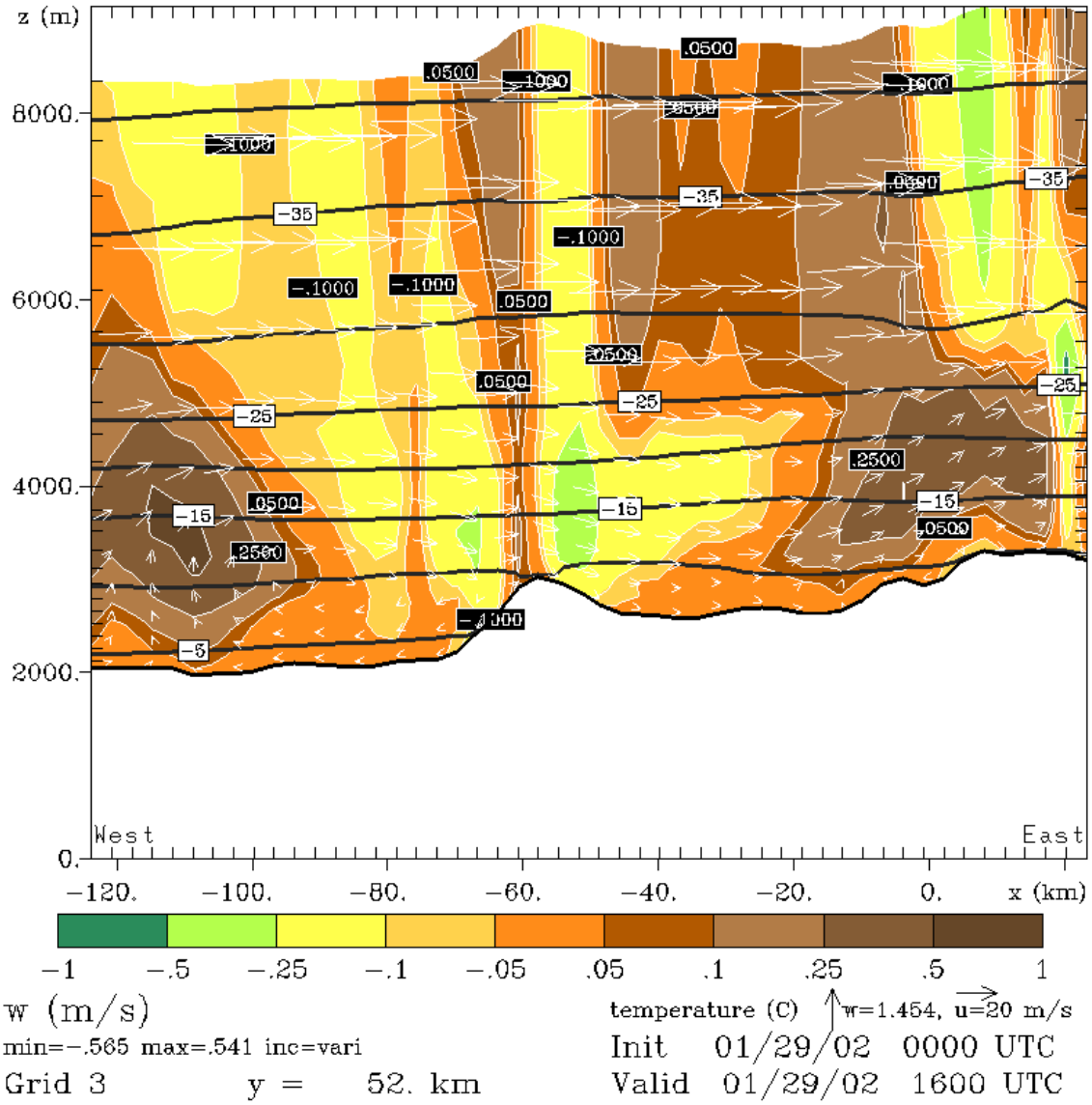

Fig. 19. RAMS model forecast of vertical velocity, temperature and winds for 16 UTC on 29 January 2002.

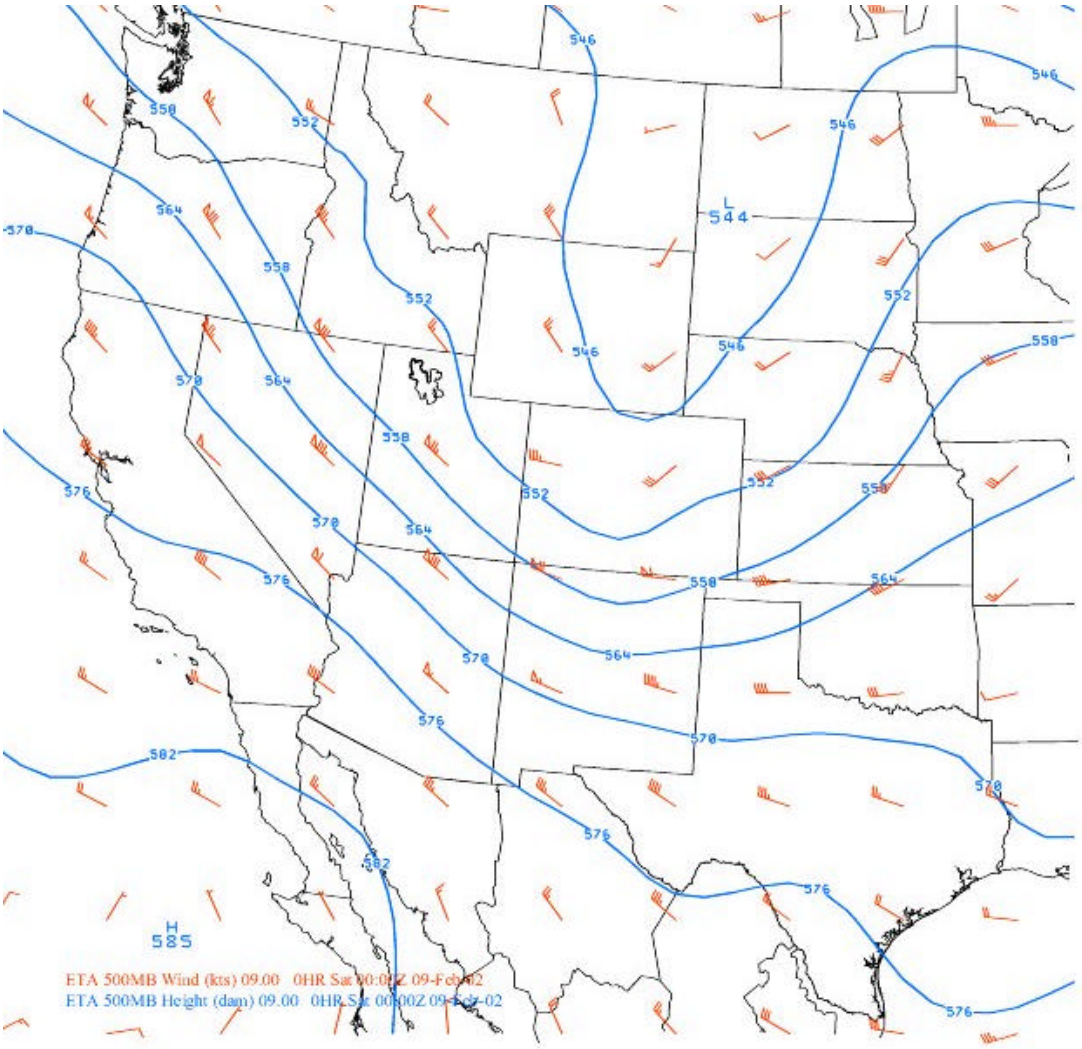

Fig. 20. ETA model 500 mb analysis of wind (kts; barbs) and height contours (dm) for 0000 UTC 9 February 2002.

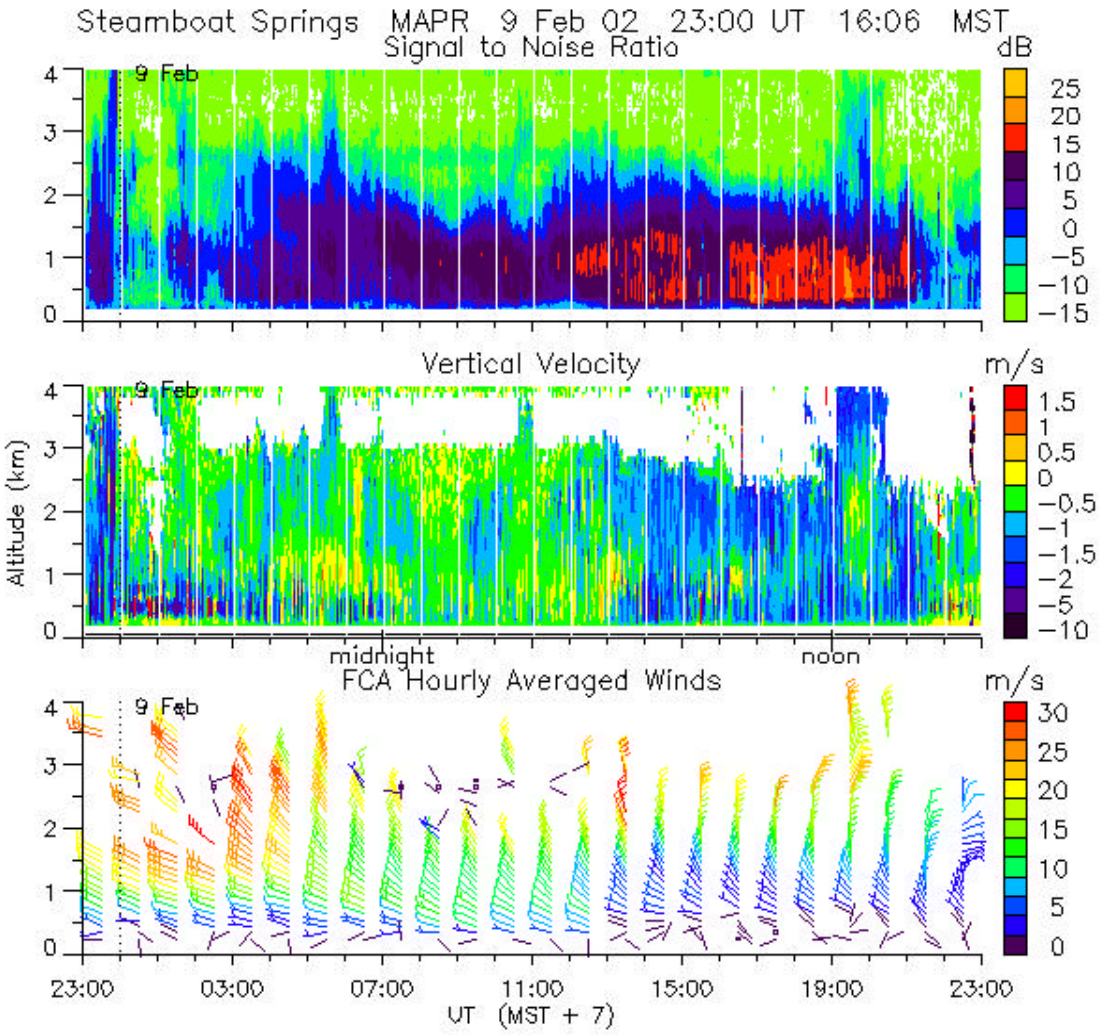

Fig. 21. NCAR MAPR radar profiles of reflectivity signal-to-noise ratio (SNR, related to precipitation intensity), vertical velocity (positive upward) and horizontal winds (upper, middle and lower panels, respectively) for 9 February 2002

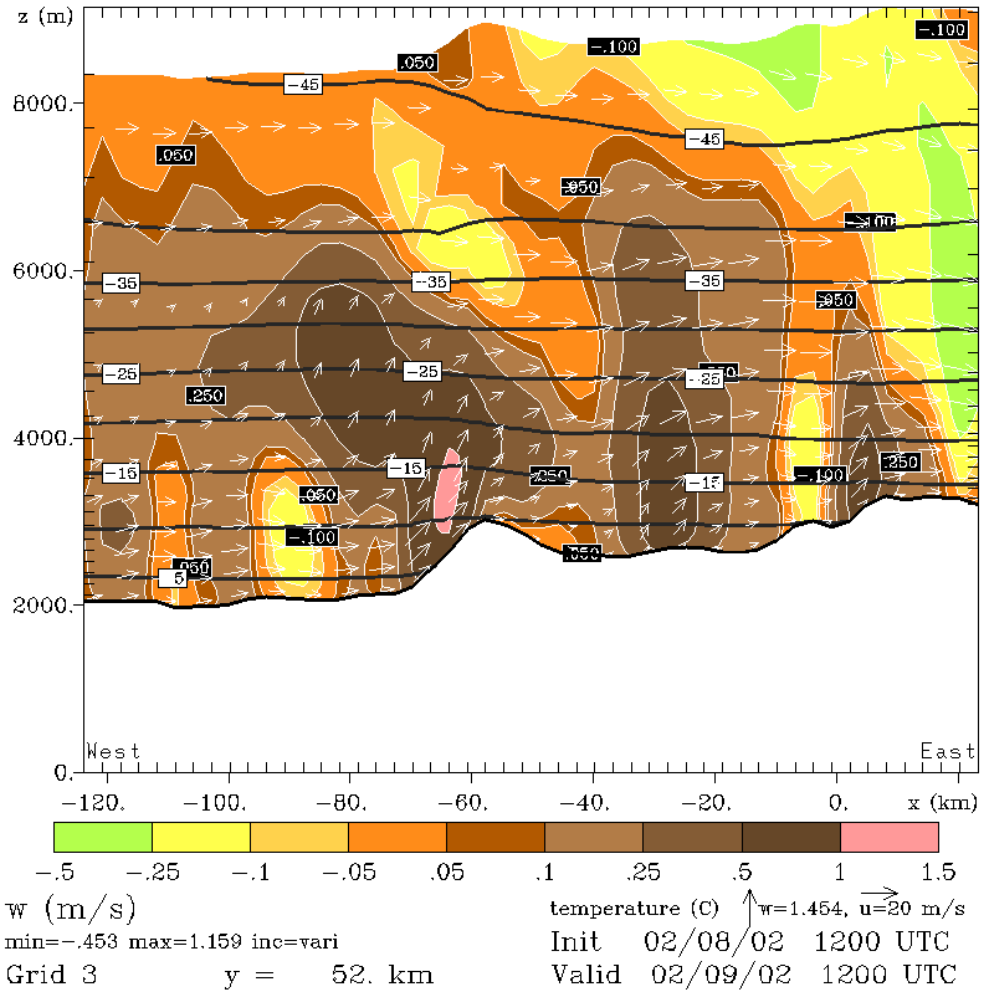

Fig. 22. RAMS model forecast cross section of vertical velocity, temperature and air motion at 12 UTC on 9 February 2002.

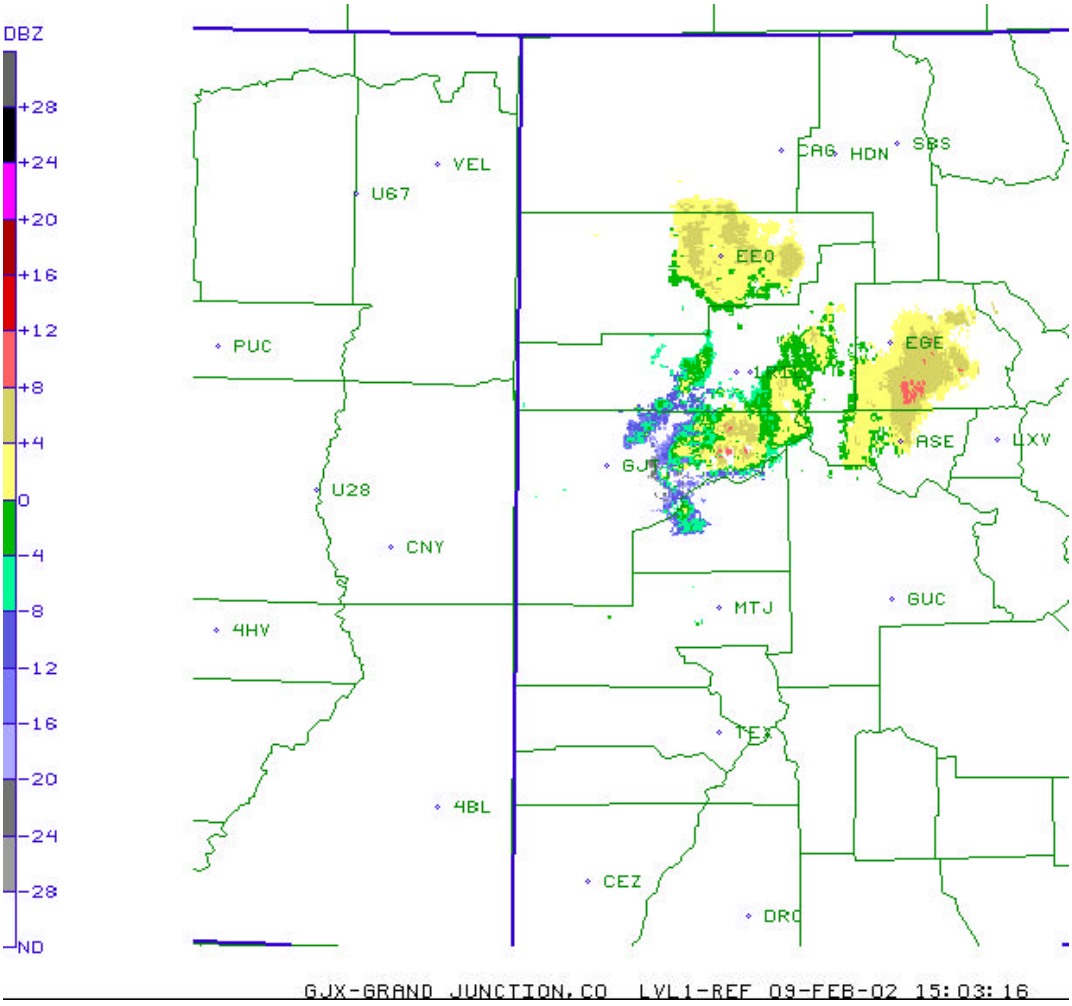

Fig. 23. NWS Grand Mesa radar reflectivity scan for 1509 UTC 9 February 2002. The scan does not reveal the snowfall occurring over the area of Steamboat Springs (SBS) and Park Range (as indicated in Fig. 21).

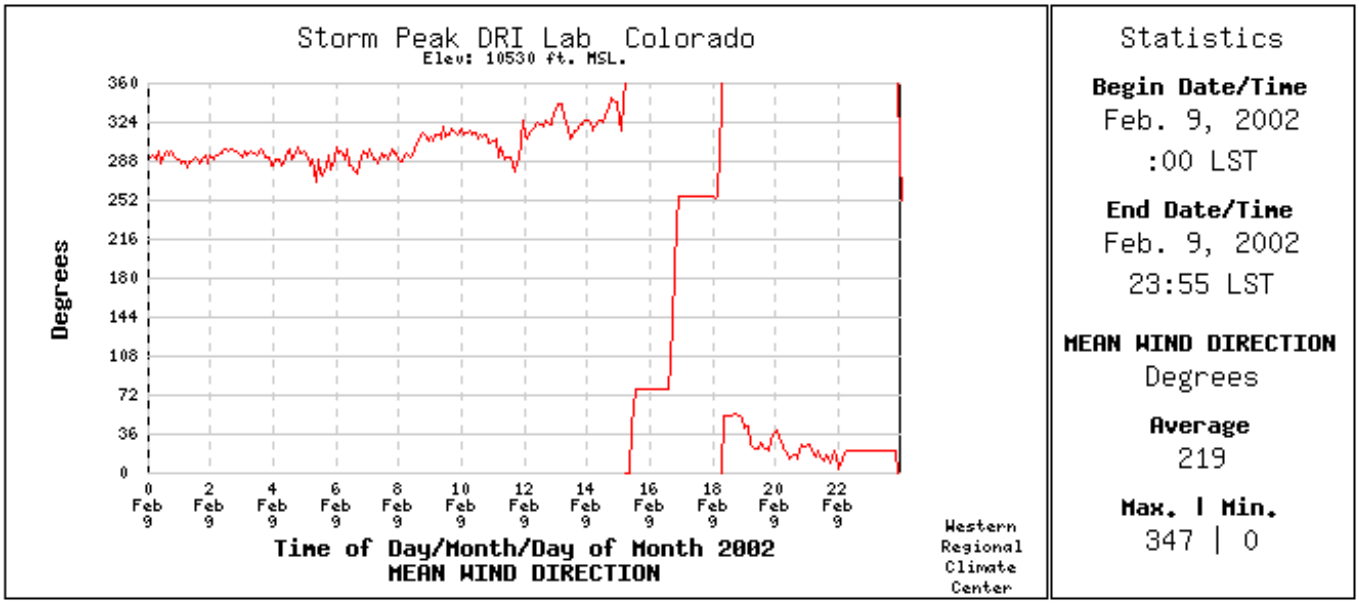

Fig. 27. Time series of wind direction measured at SPL on 9 February 2002.

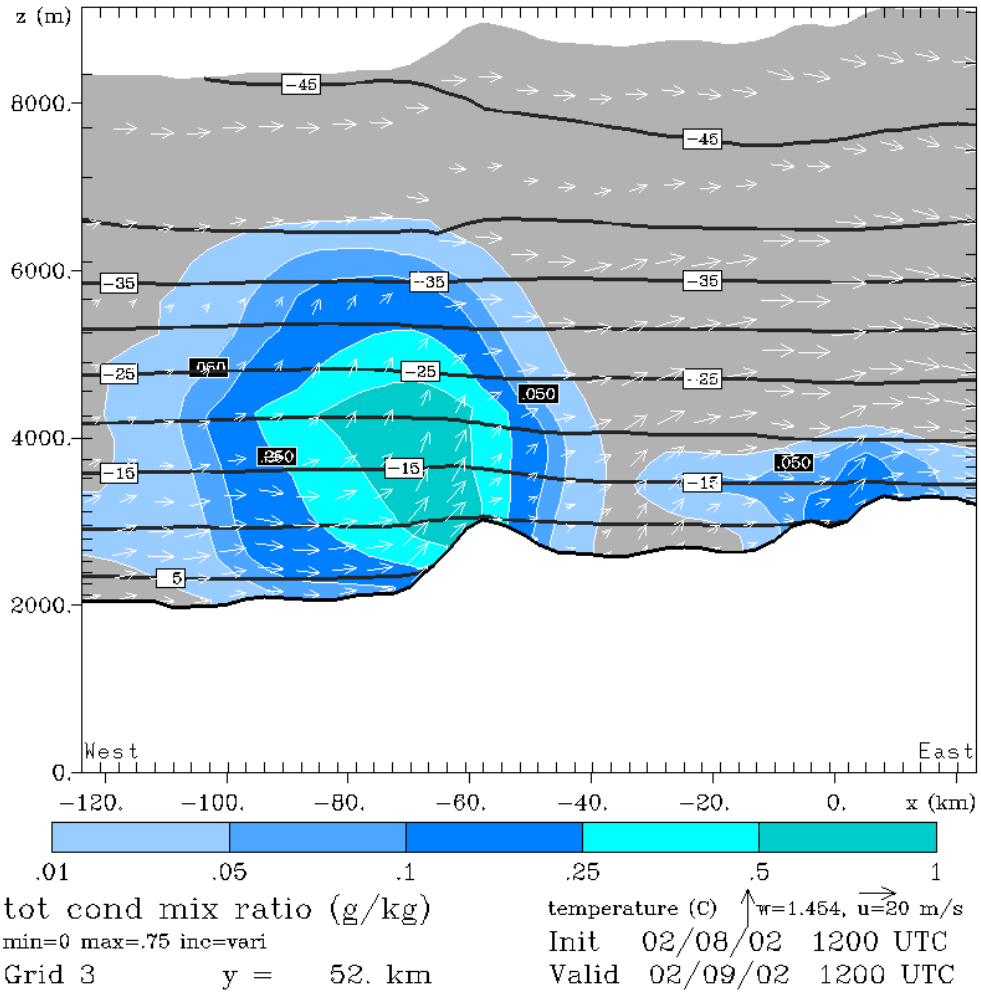

Fig. 28. RAMS model forecast of condensate (cloud + snow) mixing ratio at 1200 UTC 9 February 2002.

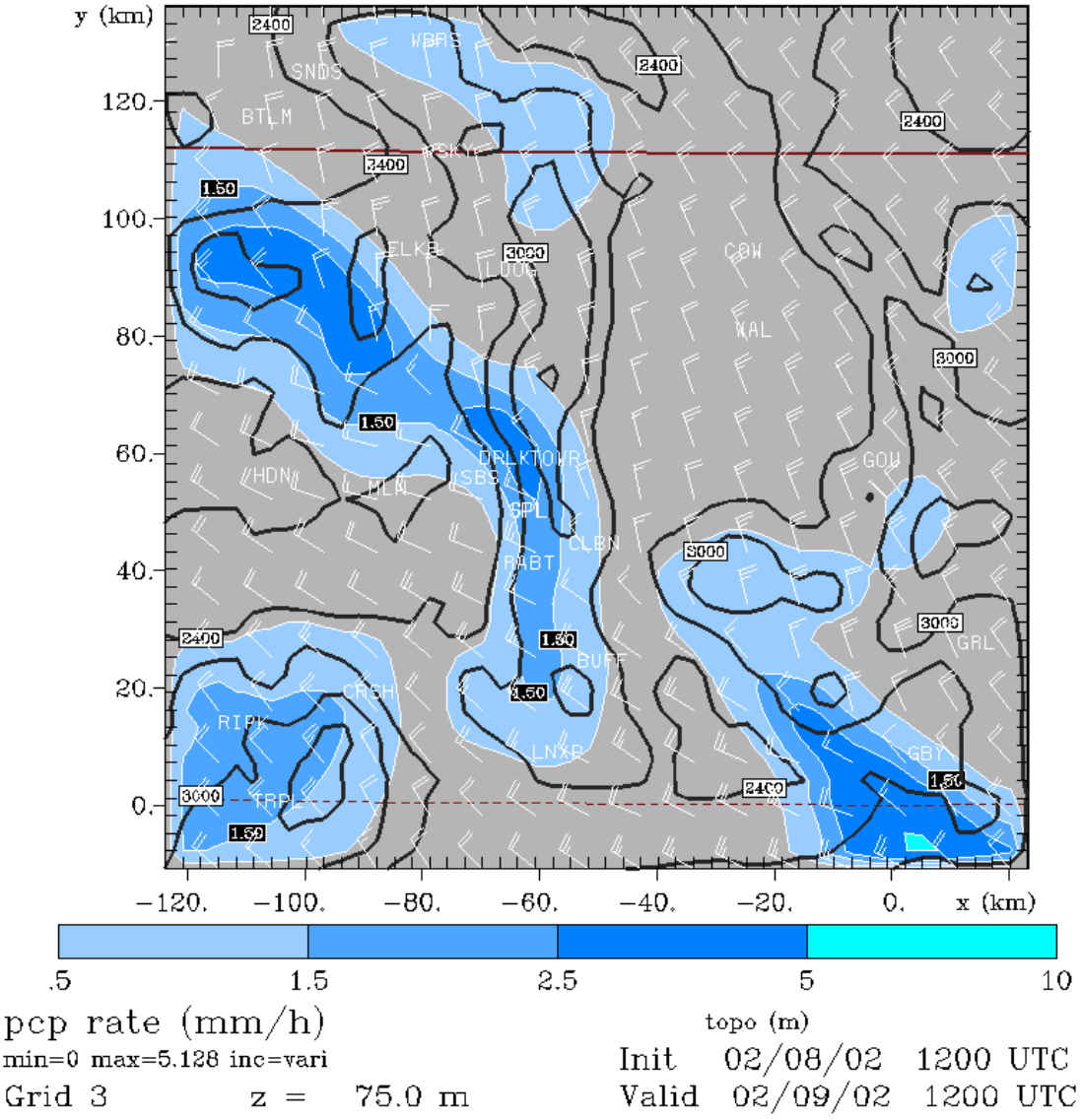

Fig. 29. RAMS model forecast of precipitation rate at 1200 UTC 9 February 2002.

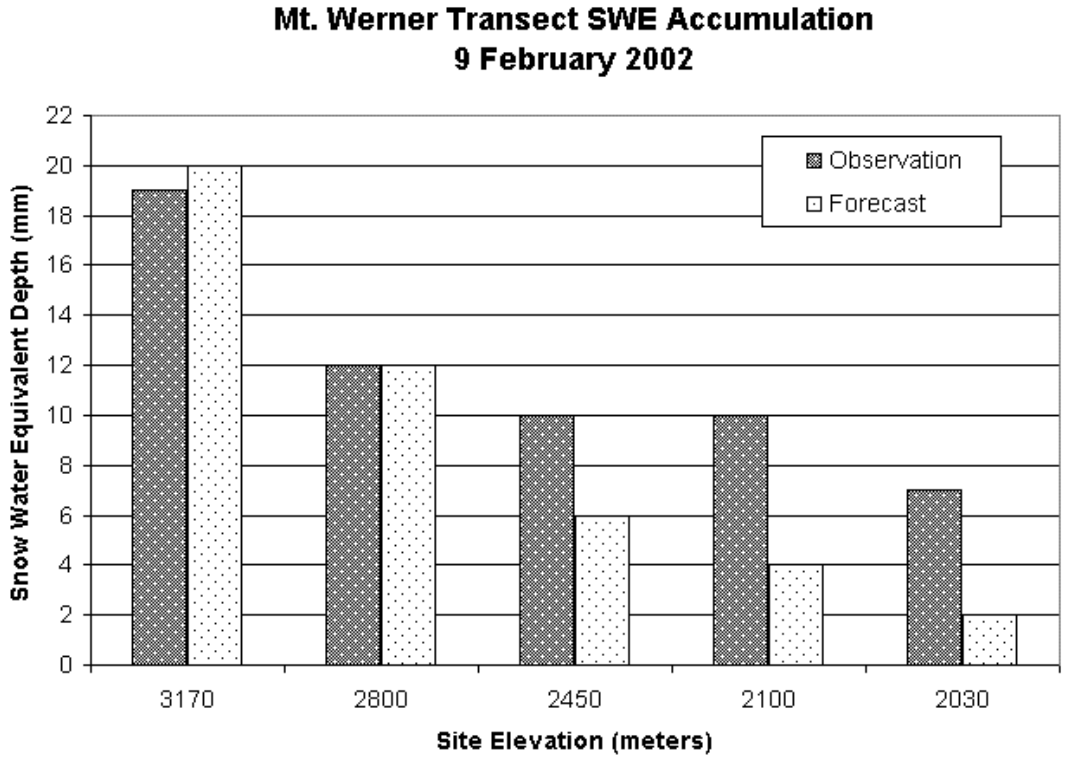

Fig. 30. Elevational comparison of observed and RAMS model forecast snow water accumulations for 9 February 2002.